Universiteit Utrecht

Investigating the interrelation of RSV infection and host cell cycle state

by

Garik Galustjan

Daily Supervisor: Dhanushika Ratnayake

Principal Investigator: Marvin Tanenbaum

Secondary Reviewer: Jop Kind

Hubrecht Institute

Universiteit Utrecht

June 2024

Abstract

Respiratory syncytial virus (RSV) infections are the leading cause of acute lower respiratory infections (ALRI) among young children and the elderly. The RSV virion contains a negative-sense single-stranded RNA genome (vRNA) that encodes eleven proteins that facilitate the propagation of the viral life cycle in infected cells. Progressing RSV infections in A549 cells are known to dysregulate the host cell cycle by inducing G1 phase arrest. Studies attempting to further investigate the patterns between of RSV infection and cell cycle progression are limited to bulk biochemical assays quantifying exclusively progressed RSV infections. We combined the intracellular vRNA visualization system RSV-P-ST/STAb-AausFP1 (P-STAb) developed by our group, with the PIP-FUCCI cell cycle reporter to generate a novel cell line (P-STAb-PIP-FUCCI$^{G/R}$). We utilized this model to monitor early and progressed RSV infections, as well as RSV entry, with the aim to examine their interrelation with the host cell cycle state and cell cycle phase durations. Our results suggest possible preferential entry for RSV virions in S phase cells and disfavored entry in G1 cells, which could likely be attributed to cell cycle-dependent RSV receptor dynamics. We noted seemingly arrested infected cells with prolonged G1 phases, however some of these cells ultimately progressed into S phase, perhaps suggesting that RSV-induced G1 arrest can be reversed. We also discovered cases of infected cells entering prolonged mitosis. Progressed RSV infections displayed significant elongations in G1 and S phase compared to their non-progressing counterparts, with a large majority of cells stalling at G1. We theorize that these cycling patterns in progressed infections are caused by a buildup of oxidative stress concomitantly induced by RSV infection.

Introduction

Epidemiological impact of RSV

Within the last 40 years, human respiratory syncytial virus (RSV) has been continuously identified as the leading pathogen contributing to the development of acute lower respiratory infections (ALRI) in children aged <5 years. (Berman 1991; Hall 2001; L. Liu et al. 2016; You 2022). In 2015, there was an estimated 33.1 million cases of RSV-associated ALRI, with approximately 59 600 in-hospital deaths and 118 200 overall deaths in children below 5 years old. About 45% of those mortalities are attributed to infants younger than 6 months (Shi et al. 2017). A follow-up review, which factored in several of emerging community surveillance studies (Srikantiah, Vora, and Klugman 2021), estimated a total of 33 million RSV-ALRI episodes in children <5 years in 2019, resulting in around 26 300 in-hospital deaths and 101 400 overall mortalities (You 2022). On top of that, RSV is considered to be a major cause of ALRI in elderly patients. A study focusing on adults aged ≥60 years living in high-income countries presented estimations of 5.2 million cases of RSV-associated respiratory infections in 2019, along with 33 000 in-hospital mortalities (Savic et al. 2023). In the US alone, the annual economic burden stemming from RSV-ALRI patients at 60 years or older has been approximated to $6.6 billion (Carrico et al. 2023), which is only projected to increase as the population continues to age.

The RSV virion

RSV is a non-segmented negative-sense single-strand RNA (-ssRNA) virus, meaning it needs to synthesize a positive-sense antigenome to use as a template for viral RNA genome (vRNA) replication and transcription. The vRNA is packaged in a lipid envelope, generally forming either spherical virions 100-250nm in diameter or filamentous particles 60-100 nm in diameter and lengths extending up to 1µm (Bächi and Howe 1973; Jeffree et al. 2003) (Figure 1B). The -ssRNA genome consists of ten genes that encode eleven separate proteins (Figure 1A). Three of these are integral transmembrane proteins: attachment glycoprotein (G), fusion (F) glycoprotein and short hydrophobic (SH) protein (Figure 1B). G protein attaches virions to target host cells through susceptible receptors, while the F protein facilitates membrane fusion (McLellan, Ray, and Peeples 2013). SH protein functions as an ion channel that has been shown to manipulate the host cell environment in a manner that inhibits host cell apoptosis, although the exact pathways it modulates are yet to be elucidated (Fuentes et al. 2007; Gan et al. 2012). The matrix (RSV-M) proteins coat the inner leaflet of the viral envelope, surrounding the vRNA. Viral nucleoproteins (N) encapsidate the vRNA, forming a helical nucleocapsid that protects the genome from degradation by cellular nucleases and serves as a scaffold for the viral replication and transcription machinery (Tawar et al. 2009). The nucleocapsid associates with phosphoproteins (P), large (L) protein and the viral transcription processivity factor M2-1 to form the viral ribonucleoprotein (vRNP)(Kiss et al. 2014). P proteins form homotetramers upon their phosphorylation, enabling them to chaperone free newly-synthesized N proteins to encapsulate nascent vRNAs. On top of that, P proteins mediate L protein attachment to the encapsidated vRNA, stabilizing the complex and acting as polymerase cofactors (Castagné et al. 2004). The L protein catalizes the replication and transcription of the vRNA, as well as the post-transcriptional processing of nascent mRNAs, such as through the addition of a 5' cap and poly-A tail (Barr and Wertz 2001; Stillman and Whitt 1999). While all of the aforementioned proteins are encoded by single corresponding genes, the M2 gene contains two partially overlapping open reading frames

(ORF) that encode for two different proteins: M2-1 and M2-2 (Collins and Wertz 1985). M2-1 regulates vRNA transcription and acts as a transcription anti-termination factor (Fearns and Collins 1999), while M2-2 plays a role in mediating the balance between vRNA transcription and replication (Bermingham and Collins 1999). The final two RSV proteins are expressed abundantly in infected cells, but are not packaged within mature virions, hence their being referred to as non-structural protein 1 (NS1) and 2 (NS2). NS1 and NS2 cooperate to form complexes that mitigate the induction of type I interferons (IFN-I) and IFN-stimulated genes (ISG), thereby suppressing the infected cell's innate antiviral response and inhibiting premature apoptosis (Bitko et al. 2007; Schlender et al. 2000). Despite the seemingly low number of proteins encoded by the RSV vRNA, their versatile interactivity and multifunctionality provide the elements necessary for successful RSV life cycle progression.

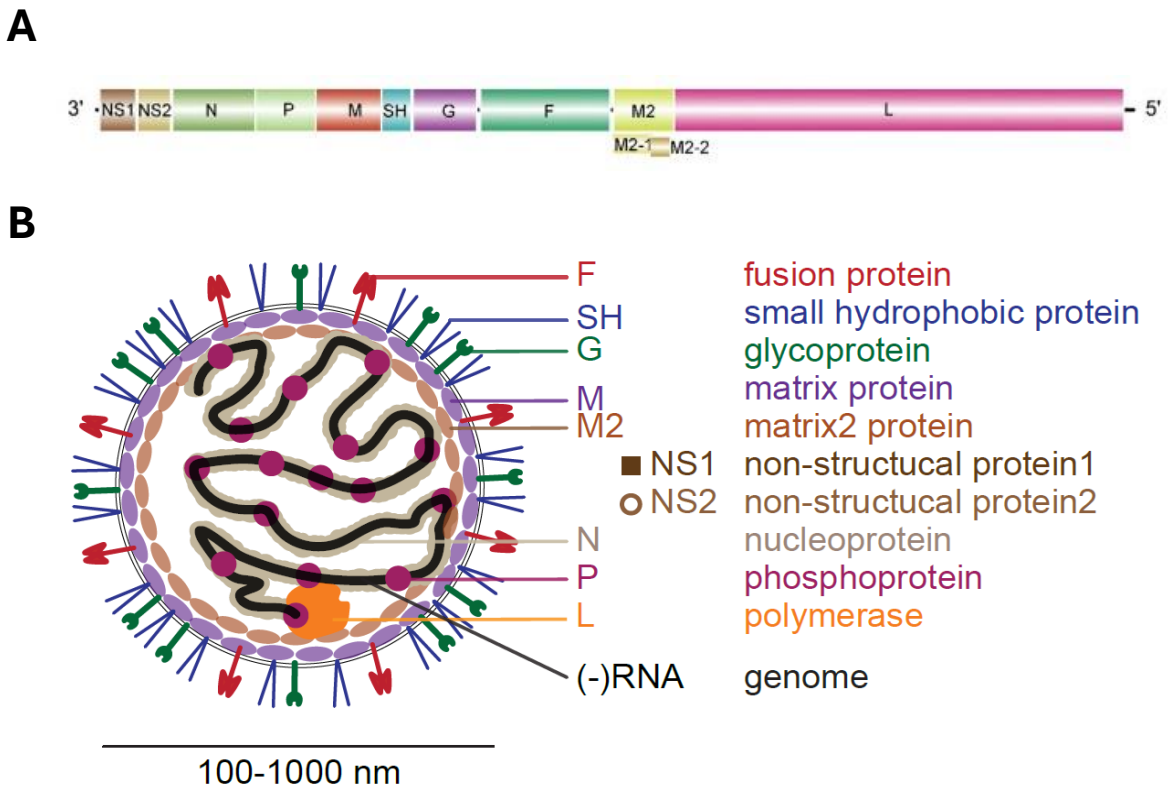

Figure 1. RSV genome and virion structure. (A) *The RSV genome consists of 11 open reading frames (ORF), encoding for non-structural proteins (NS1 & NS2), nucleoprotein (N), phosphoprotein (P), matrix (M) protein, small hydrophobic (SH) protein, glycoprotein (G), fusion (F) protein, M2-1, M2-2 and polymerase (L) protein. Adapted from (Shang, Tan, and Ma 2021).* ***(B)*** *Composition of the RSV virion and the general distribution of its viral proteins. NS1 and NS2 are not packaged in the viral particle. Human RSV virions generally present with spherical or filamentous morphologies, between 100 and 1000nm in length. Adapted from (Boersma 2022).*

The RSV life cycle

RSV infection begins with viral entry, which involves the virion-host cell attachment and fusion, orchestrated by the G and F proteins respectively (Figure 2). Both glycoproteins interact with the target cell through a range of specific receptors. G protein can bind heparan sulphate proteoglycans (HSPG) (Krusat and Streckert 1997), which seem to strongly promote RSV infection in immortalized cell lines (Hallak, Collins, et al. 2000; Martinez and Melero 2000). However, HSPGs are shown to be scarcely expressed on the apical membranes of primary human bronchial

epithelial (PHBE) cells, one of the main primary cell types associated with RSV infections (Duan et al. 1998; Hallak, Spillmann, et al. 2000; Zhang et al. 2002). G proteins contain a CX3C motif, which allows them to bind to CX3C chemokine receptor 1 (CX3CR1) through chemokine mimicry (Tripp et al. 2001). Additionally, CX3CR1-G protein interaction was shown to mitigate the antiviral immune response against infected cells, mainly by suppressing the induction of IFN-γ (Harcourt et al. 2006). Following cell attachment, RSV F can bind to host surface receptors to mediate the process of membrane fusion. More specifically, F protein has been shown to interact with intercellular adhesion molecule-1 (ICAM-1), epidermal growth factor receptor (EGFR), nucleolin (NCL) and insulin-like growth factor-1 receptor (IGF1R). EGFR, ICAM-1 and NCL have all been directly implicated in mediating virion macropinocytosis (Krzyzaniak et al. 2013; Patel et al. 1995; Tayyari et al. 2011), whereas IGF1R binds F proteins to activate protein kinase C zeta (PKCζ), triggering a signalling cascade that facilitates the translocation of nuclear NCL to the cell membrane, further augmenting RSV internalization (Griffiths et al. 2020).

Upon entry, the RSV nucleocapsid is released into the cytosol, along with all other viral proteins contained in the envelope. L and P proteins form the RNA-dependent RNA polymerase complex (RdRp), which mediates both genome replication and viral mRNA transcription, jointly regulated by M2-1 and M2-2 (Figure 2). The resultant vRNPs aggregate within liquid-liquid phase separated cytoplasmic inclusion bodies (IB). IBs are often described as viral factories, harboring invading vRNPs and drastically amplifying infection progression by facilitating active vRNA replication and transcription (Garcia-Barreno, Delgado, and Melero 1996). vRNA replication involves the generation of a full-length positive-sense copy of the genome, called the antigenome, which in turn serves as the template for the synthesis of new negative-sense vRNAs. vRNA transcription results in the production of subgenomic mRNAs that are translated by host cell ribosomes into functional viral proteins. In early infection stages, newly-synthesized vRNP-associated proteins are contributed back into the transcription and replication cycles, thereby establishing positive feedback loops that exponentially expand the manufacture of vRNPs. Simultaneously, RSV-M proteins are temporarily transported to the nucleus, where they generally inhibit host cell transcription (Ghildyal et al. 2003). NS1 and NS2 monomers can bind and functionally inhibit certain pattern recognition receptors (PRR), e.g. retinoic acid-inducible gene I (RIG-I), or combine to form degradasome complexes that degrade various effectors of the IFN-I signaling cascade (Elliott et al. 2007; Ling, Tran, and Teng 2009; Swedan, Musiyenko, and Barik 2009). As host cell infection progresses, synthesized G, F, SH and RSV-M proteins are shuttled to the cell membrane, seemingly concentrating in lipid-raft rich regions (Jeffree et al. 2003). Once the cell is primed for the assembly of new virions, vRNP complexes are transferred to the cell periphery, where they may interact with membrane-associated RSV-M proteins to initiate virion budding (Ke et al. 2018). The released viral progeny continues to propagate the RSV infection cycle by infecting neighbouring cells.

Effects of virus infection on cell cycle

Viruses are known to hijack cellular machinery and systematically manipulate the host cell environment in order to optimize their replication prospects, which may entail host cell cycle dysregulation. The eukaryotic cell cycle can be divided into two main stages: mitosis (M), where cells are duplicated into two identical daughter cells, and interphase, where cell undergo multiple phasic processes to prepare for mitosis. Phase progression is robustly controlled by sequentially activated families of cyclins and cyclin-dependent kinases (CDK). In early interphase,

cyclin D-bound CDK4 and CDK6 drive the cell into G1 phase, where it grows in size and synthesizes more proteins and mRNA in preparation for DNA replication (Sherr 1994). After some time, cyclin E binds CDK2 to promote transition from G1 to S phase, where DNA synthesis is stimulated by the cyclin A-CDK2 complexes (Girard et al. 1991; Ohtsubo et al. 1995). After S phase, the cell will transition to G2 phase, where it prepares for mitosisIn late G2, cyclin A will interact with CDK1 to promote mitosis initiation, while cyclin B-associated CDK1 regulates M progression and completion (King, Jackson, and Kirschner 1994). Following mitotic cell division, the resultant daughter cells enter G1 phase, thereby marking the start of a new cycle. Cell integrity during the cycle is overseen by three checkpoints stationed at the G1/S and G2/M junctions, as well as in the middle of mitosis, which can prompt cell cycle arrest or p53-dependent apoptosis in response to DNA damage (Fernandez-Capetillo et al. 2002; Gottlieb and Oren 1998; Musacchio and Salmon 2007; Pardee 1974). Studies investigating the interrelation between viral infection and host cell cycle state determined that viruses often incite arrest at specific cell cycle stages or disparately overturn checkpoint-induced arrest (Bagga and Bouchard 2014).

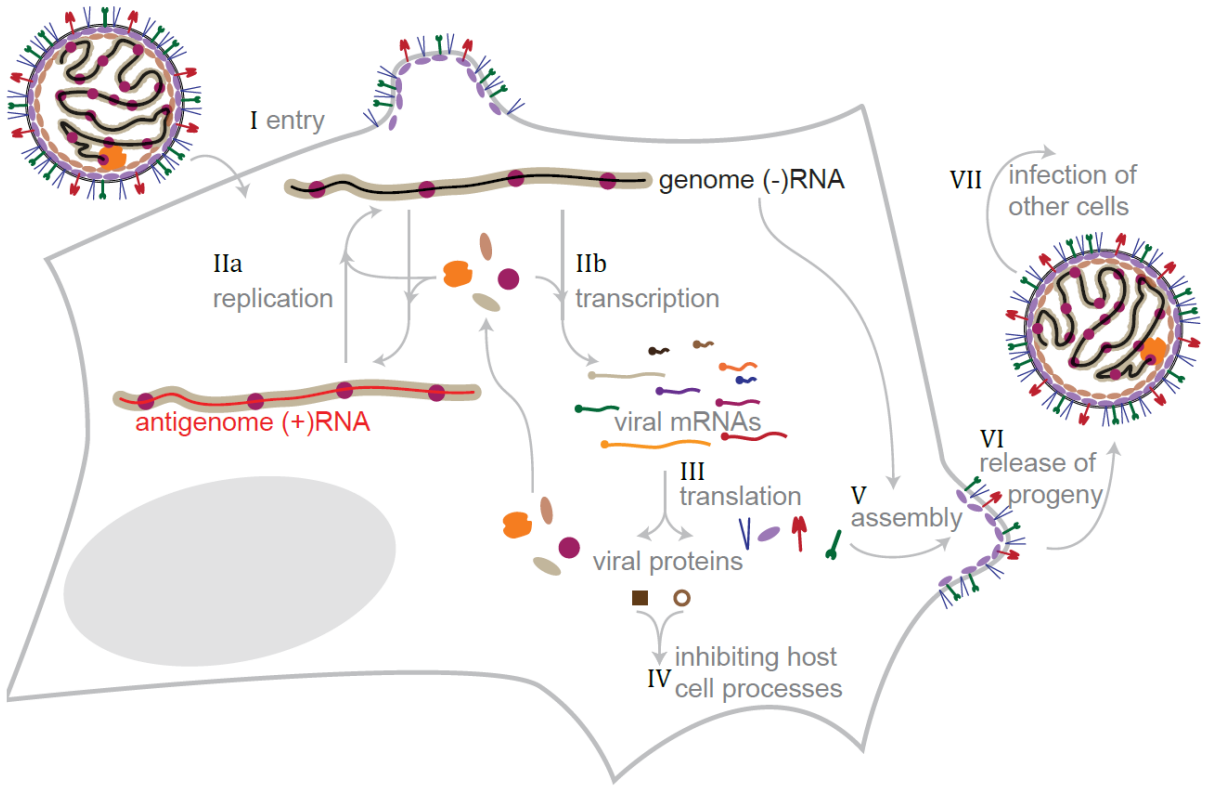

Figure 2. RSV life cycle. *RSV virion surface glycoproteins bind to host cell receptors and fuse to the host cell membrane (I), releasing the viral genome and proteins into the cytosol. The viral proteins facilitate -RNA genome replication (IIa), by producing +RNA antigenomes to be used as templates for -RNA genome synthesis, and viral mRNA transcription (IIb). Viral mRNAs are translated (III) by host cell ribosomes. Newly synthesized viral proteins contribute to infection progression by further promoting viral transcription and replication, inhibiting host cell processes like innate immune recognition (IV) and priming the cell membrane for the assembly of new virions (V). In later infection stages, RSV progeny will bud from the host cell (VI) and go on to infect neighbouring susceptible cells (VII). Adapted from (Boersma 2022).*

As an example, the +ssRNA severe acute respiratory syndrome coronavirus 1 (SARS-CoV-1) has been shown to induce G1 arrest in infected cells through the action of its nonstructural proteins 3b and 7a (Yuan et al. 2005, 2006). Interestingly, the method of cell cycle dysregulation is not consistent among members of the same virus families, as SARS-CoV-2 infections precipitated arrest in the S and G2 phases (Suryawanshi et al. 2021). Evidence suggests that virus-induced effects on cell cycling can be strictly cell type-specific. For instance, hepatitis B virus (HBV) infection in HepG2.2.15 cells leads to G1 arrest (T. Wang et al. 2011), while HBV infections in Huh7 cells lead to stalls in G2 phase (Chin et al. 2007). Small DNA tumour viruses, such as human papillomavirus (HPV), can force cells to bypass G1 checkpoint arrest by inhibiting the expresson of tumor-suppressing retinoblastoma protein (Rb) and forcedly driving infected cells into S phase (Bourgo et al. 2009). Since HPV does not encode its own DNA polymerase, this process allows it to efficiently hijack the host DNA replication machinery and initiate viral genome replication (Helt and Galloway 2003).

Focusing on the realm of -ssRNA viruses, RSV infection has been shown to induce G1 arrest in adenocarcenomic lung epithelial (A549) cells and primary human bronchial epithelial (PHBE) cells, through increased activation of p53. p53 upregulates the expression of CDK inhibitor p21, which inhibits the kinase activity of CDK2 and halts the G1/S transition step (Harper et al. 1995). The exact method of p53 activation employed by the virus is yet to be elucidated, however this overactivation has been linked to the host cell transcriptional alterations induced by RSV-M (Bian et al. 2012). Furthermore, NS1 has been shown to activate transcription factor Kruppel-like factor 6 (KLF6), which positively regulates the expression of transforming growth factor-β (TGF-β) and triggers TGF-β-dependent G1 arrest (Bakre et al. 2015; Laiho et al. 1990). Influenza A virus (IAV) parallels RSV in inducing G1 arrest through the action of its respective M and NS1 proteins, although the mechanisms they target differ slightly from their RSV-counterparts (Jiang et al. 2013; Zhu et al. 2021). On the other hand, Ebola virus (EBOV)-infected epithelial cells displayed accelerated cell cycling and a breakdown in cell cycle checkpoints, following an upregulation of cyclin D1 triggered by the EBOV matrix protein VP40 (Pleet et al. 2018). These varied forms of cell cycle dysregulation are theorized to provide optimal conditions for viral replication and aid infection progression, whether it be through the immune evasion inherent in arrested cells or through the enhanced production of viral progeny granted by checkpoint blockade (Bagga and Bouchard 2014).

Limitations in examining the interrelation between virus infection and cell cycle

The discussion concerning the interrelation of host cell cycle and viral infection remains largely speculative, as evidence outlining the interplay between the two processes is lacking. Most studies centered on this topic employ bulk biochemical assays to present correlations between viral protein expression and the activation/inactivation of cell cycle regulators, omitting the viral and host heterogeneity that impacts infection dynamics (Jones, Le Sage, and Lakdawala 2021). Some groups have utilized the fluorescence ubiquitination cell cycle indicator (FUCCI) to investigate virus-induced cell cycle alterations at a single-cell level. The reporter is comprised of mKO2 and mAG fluorophores fused to ubiquitin ligase substrates Cdt1[30-120] and Geminin[1-110] (Gem[1-110]) respectively, the expression of which is regulated through the cell cycle-dependent proteolysis of their respective E3 ligases: SCF^{Skp2} and anaphase-promoting complex (APC^{Cdh1}). mKO2-Cdt1[30-120] levels accumulate throughout G1 phase, illustrated by red nuclear fluorescence, but become degraded by SCF^{Skp2} once the cell transitions into S

phase. Correspondingly, the start of S phase is marked by increasing levels of mAG-Gem[1-110], depicted by green nuclear fluorescence, which continue to accumulate until the subsequent G1 phase, at which point the fusion protein is rapidly broken down by APC^{Cdh1}. The inversely oscillating levels of these fluorescent probes allow for the demarcation of G1 and S/G2 phases in single cells through flow cytometry or fluorescence microscopy (Sakaue-Sawano et al. 2008). As an example, a recent study examining A549 cells infected with SARS-CoV-2 utilized FUCCI to track the degradation of cyclin D3 at various cell cycle phases, determining that SARS-CoV-2-induced S/G2 arrest is independent of cyclin D3 depletion (Gupta and Mlcochova 2022). Although FUCCI allows for distinct delineation of specific cell cycle phases in live cells without the need for exogenous treatment, its inability to demarcate the full range of the S and G2 phases individually is a major drawback. Besides that, this field lacks reliable methods for tracking viral entry, as well as visualizing the early stages of viral transcription and replication, which leaves major gaps in our understanding of the interplay between cell cycle and viral infection.

To address these limitations, our group has generated a cell line expressing an engineered RSV P protein carrying a single repeat of SunTag (P-ST), which is a peptide array that serves as a scaffold for the binding of intracellularly-expressed SunTag antibodies labelled with green fluorophore AausFP1 (STAb-AausFP1) (Tanenbaum et al. 2015). The binding of numerous P-ST fusion proteins, and their associated STAb-AausFP1 (P-STAb), allows for the visualization of individual RSV nucleocapsids via the principle of fluorophore multimerization. Hence, the P-STAb toolkit permits the tracking of RSV infections from the point of initial entry to the development of late-stage infection. Furthermore, a recently developed variant of the FUCCI sensor, referred to as PIP-FUCCI, improves upon the original by permitting the precise delineation of each cell cycle phase (Grant and Kedziora 2018). Specifically, it replaced the Cdt1[30-120] expression construct with the Cdt1[1-17] sequence, which produces a PCNA-interaction protein (PIP) degron. PIP binds proliferating cell nuclear antigen (PCNA) throughout S phase, which is when it is actively degraded by Cullin4 RING ligase ($CRL4^{Cdt2}$). However, PIP begins to reaccumulate once the cell enters G2 phase, thereby accurately delineating the G1/S and S/G2 cell cycle transitions through its expression. PIP was fused to a nuclear localization sequence (NLS), a human influenza hemagglutinin (HA) tag and an mVenus fluorophore (PIP-mVenus), while Gem[1-110] was fused to mCherry (Gem[1-110]-mCherry). The expression constructs were linked via a P2A peptide sequence to ensure ratiometric expression of the fusion proteins. The resultant PIP-NLS-mVenus-P2A-mCherry-Gem[1-110] ($PIP\text{-}FUCCI^{G/R}$) construct improves upon the original FUCCI sensor, by accurately demarcating all cell cycle phase transitions and permitting reliable cell cycle phase identification (Grant and Kedziora 2018).

The cornerstone of this project was the combined application of the P-STAb system and the PIP-FUCCI reporter to examine the interplay between early RSV infection and host cell cycle at a single-cell resolution. Employing this combinatorial approach, we aimed to systematically investigate whether early and progressed RSV infections, as well as the incidence of RSV entry, can be linked to specific cell cycle phases or alterations in cell cycle progression.

Methods

Cultured cell lines

A549 cells were utilized for cell cycle analysis and RSV infection experiments. HEK293T cells were employed for lentivirus production. All cells were cultured in Dulbecco's Modified Eagle Medium (DMEM)(Gibco; Waltham, MA, USA), supplemented with 1% penicillin/streptomycin (Gibco) and 10% fetal bovine serum (FBS) (Sigma-Aldrich; St. Louis, MO, USA). Cells were grown at 37°C with 5% CO_2.

Reporter cell line generation

All the cell lines utilized through the course of this project, whether obtained or generated, are outlined in Table 1. The HaloTag self-labelling protein tag was utilized to detect cells positive for P-ST expression (Los et al. 2008).

Plasmids

PIP-NLS-mVenus-P2A-mCherry-Gem[1-110] (PIP-FUCCI$^{G/R}$) plasmid was purchased from the Jean Cook Lab through the Addgene repository (Addgene; Watertown, MA, USA; Cat. #118616)(Grant and Kedziora 2018). STAb-AausFP1 and HaloTag-P2A-RSV-P-ST (HALO-P-ST) plasmids were previously produced by our group.

Cell line	Source	Plasmid Identifier
A549 wildtype	Rameix-Welti Lab (Institut Pasteur)	N/A
HEK293T	Tanenbaum Lab (Hubrecht Institute)	N/A
PIP-FUCCI$^{G/R}$ + PIP-NLS-mVenus-P2A-mCherry-Gem[1-110]	Generated for this study	Addgene Cat. # 118616
P-STAb-PIP-FUCCI$^{G/R}$ + PIP-NLS-mVenus- P2A-mCherry-Gem[1-110] + STAb-AausFP1 + HaloTag-P2A-RSV P-ST	Generated for this study	Addgene Cat. # 118616 N/A N/A
P-STAb-PIP-FUCCI$^{R/B}$ + PIP-NLS-mCherry- P2A-BFP-Gem[1-110] + STAb-AausFP1 + HaloTag-P2A-RSV P-ST	Generated for this study	 N/A N/A N/A

Table 1. *An outline of all the cell lines utilized in this study, including where they were obtained from, which transgenes they express and their corresponding plasmid catalogue numbers, where applicable.*

To generate PIP-NLS-mCherry-P2A-BFP-Gem[1-110] (PIP-FUCCI$^{R/B}$), pHR-mCherry plasmid (Tanenbaum Lab; Cat. #422) was linearized with restriction endonuclease BamHI-HF (New England Biolabs; Ipswich, MA, USA) and CutSmart Buffer (New England Biolabs) according to manufacturer's specifications. The linearized plasmid was isolated with the use of a GeneJET gel extraction kit (Thermo Fisher Scientific; Waltham, MA, USA). An 188bp insert containing sequences for PIP and NLS was obtained from the PIP-NLS-mVenus-P2A-mCherry-Gem[1-110] template through Q5 High-fidelity polymerase chain reaction (PCR) (New England Biolabs) with primers 35-Cdt1-F and 36-Cdt1-R (Table 2). The backbone and insert sequences were fused through Gibson assembly to generate

PIP-NLS-mVenus.(Gibson et al. 2009) Successful clones were selected through colony PCR and verified through sequencing. PIP-NLS-mVenus was then linearized with restriction enzyme NdeI (New England Biolabs). pHR-Tet3G-P2A-BFP (Tanenbaum Lab; Cat. #564) and pHR-BFP-Gem-NLS (Tanenbaum Lab; Cat. #469) plasmids were used as templates to obtain inserts P2A-BFP (812bp) and Gem[1-110] (392bp) (primers outlined in Table 2). The inserts were combined into a single sequence through fusion PCR and joined with the PIP-NLS-mVenus vector backbone through Gibson assembly. Successful insertion was verified through sequencing. Ampicillin resistance was used for bacterial selection.

Primer title	Primer sequence	Primer direction
35-Cdt1-F	GTACGGCCACCATGCGatggagcagcgccg	5'-3'
36-Cdt1-R	ccttgctcacGGATCCactagttgcatagt	3'-5'
37-P2A-BFP-F	acaagCGGTCCGACAACGGAAGCGGAGCTA	5'-3'
38-P2A-BFP-R	GGCCGCGCCACCACCACCATTAAGCTTGTG	3'-5'
39-Gem_1-110-F	GGGCACAAGCTTAATGGTGGTGGTGGCGCG	5'-3'
40-Gem_1-110-R	GCGCTCAGCATCATATGTTACAGCGCCTTT	3'-5'

Table 2. *List of primers utilized for PCR and sequencing.*

Bacterial transformation

DH5α competent E. coli cells initially stored at -80°C were thawed on ice for 5 minutes. A minimum of 200ng of plasmid DNA was added directly to the cells and mixed gently through tapping. Bacteria and plasmids were incubated on ice for 15 minutes, after which they were exposed to a 42°C heat-shock for 45 seconds, followed by a further 2-minute incubation on ice. 300µL of Luria broth (LB) was added to the transformed bacteria and the mixture was kept in an incubator shaker for 1 hour at 37°C 200 RPM. After that, 150µL of the mixture was transferred to LB-agar culture plate containing Ampicillin (LA+Amp), spread evenly with a cell spreader and incubated at 37°C overnight. The following day, individual colonies were picked and inoculated into separate cell culture tubes containing 4mL of LB supplemented with Ampicillin (1:1000). The tubes were left in an incubator shaker at 37°C 200 RPM over 24 hours to promote bacterial growth. Plasmid DNA was isolated using a GeneJET plasmid Miniprep Kit (Thermo Fisher Scientific) according to the protocol provided by the manufacturer. Successful plasmids were verified by sequencing.

Lentivirus production

1µg of purified lentiviral plasmid DNA was mixed with 0.4µg of pMD2.G and 0.6µg of pspax2 packaging vectors and transfected into HEK293T cells using polyethylenimine (PEI) transfection reagent. The plasmids were added to 10µL of PEI and 50µL of Opti-MEM medium (Thermo Fisher Scientific), mixed by pipetting and incubated the room temperature (RT) for 5-15 minutes. The transfection mix was added directly to the culture medium of HEK293T cells grown to 50-60% confluency in a 6-well plate. After 24 hours, the transfection efficiency is determined through an EVOS FL fluorescence microscope (Thermo Fisher Scientific) and the culture medium is refreshed with

DMEM/. Following 48 hours, assuming ~100% of the cell are fluorescent, the lentivirus-containing supernatant is collected and either utilized immediately or stored at -80°C for future use.

Lentiviral transduction

Stable, transgene-expressing A549 cell lines were generated through lentiviral transduction. A549 cells are grown to ~50% confluency in a 6-well plate. They are infected with a mix containing 300µL of DMEM/=, 300µL of lentivirus and 1µL of Polybrene (10mg/mL) (Santa Cruz Biotechnology; Dallas, TX, USA). Cells were spin-infected for 120 minutes at 2000 RPM at RT. The virus-containing medium is then aspirated, the cells are washed once with medium and cultured normally for at least 2 passages prior to freezing or sorting. Transgene expression was confirmed with spinning-disk confocal microscopy. Cell lines expressing multiple transgenes were transduced sequentially. Polyclonal cell lines were sorted into monoclones according to expression intensity of fluorescent tags through fluorescence-activated cell sorting (FACS) using the Fusion flow cytometer (BD BioSciences; Franklin Lakes, NJ, USA).

Cell cycle analysis by DAPI staining

DAPI nuclear staining was utilized to orthogonally confirm the accuracy of the PIP-FUCCI system for cell cycle phase delineation. A549 and A549-PIP-FUCCI(mV/mCh) cells grown to ~40-50% confluency in 6-well plates were treated with either 1µM Palbociclib (Selleck Chemical; Houston, TX, USA) or dimethyl sulfoxide (DMSO) as a treatment control. After 24 hours, the culture medium is collected to preserve mitotic cells and the adhered cells are detached with TryplE. The trypsinized and mitotic cells are spun down together for 5 minutes at 1500 RPM to form a pellet, which are the settings utilized for all pelleting steps in this protocol. The resultant pellet is resuspended in PBS and pelleted again. The cells are then resuspended in 500µL of 4% paraformaldehyde (PFA) (Thermo Fisher Scientific) and incubated for 10 minutes at RT on a tube rotator. The fixed cells are spun down, washed with PBS and spun down again, after which they are permeabilized with 500µL of 0.2% Triton X-100 (Sigma-Aldrich) at RT for 10 minutes. Permeabilized cells are pelleted, resuspended with 200µL of PBS containing 0.25µg/mL of DAPI and incubated at RT for 15 minutes while wrapped in aluminium foil. The samples are spun down one last time to wash out excess DAPI, respuspended in 500µL of PBS and pipetted through blue filter FACS tubes (Corning Inc.; Corning, NY, USA) to isolate single cells. Sample fluorescent signatures were obtained using the CytoFLEX S flow cytometer (Beckman Coulter; Brea, CA, USA) and analyzed with the CytExpert software package (Beckman Coulter).

Virus strain

Cells were infected with WT human RSV Long strain, group A.

Live cell imaging

Treatment and infection for imaging

All cells were plated on 96-well square glass-bottom plates (Ibidi; Gräfelfing, Germany) at least 1 day prior imaging. 30-60 minutes prior to imaging, any culture medium in the plates was replaced with Leibovitz's L-15 Medium (Gibco), supplemented with 10% FBS. Surrounding wells were filled with PBS to mitigate medium evaporation. A549-PIP-FUCCI(mV/mCh) cells were treated SiR-Hoechst (1:1000) (SpiroChrome; Stein am Rhein, Switzerland) and verapamil (1:2000) (SpiroChrome) for live cell nuclear staining 2 hours prior to imaging. Cells expressing HALO-P-ST were incubated with HaloTag ligand Janelia Fluor 646 (JF646) (Promega; Madison,WI, USA) for 15-30 minutes at 37°C. Cells were then exposed to two 15-minute washes and 2 quick washes with DMEM, after which they were imaged. WT RSV was diluted in L-15 imaging medium to obtain multiplicities of infection (MOI) ranging between 0.25-0.6 upon cell infection. Fluorescently labelled RSV G antibody (Novus Biologicals; Minneapolis, MN, USA; Cat. # NBP2-50411JF646) was added directly to imaging medium at 1:1000 dilution.

Spinning disc confocal microscopy

All fluorescent imaging was carried out on a Nikon ECLIPSE TI2 series inverted microscope (Nikon; Tokyo, Japan) coupled with the Yokagawa CSU-X1 confocal field scanning spinning disc system (Yokogawa Electric; Tokyo, Japan) and a Prime 95B sCMOS camera (Teledyne Photometrics; Tucson, AZ, USA). Images were acquired with a ×60/1.40 NA oil-immersion objective through the NIS-Elements software (Nikon). For Z-stack timelapse acquisition, the built-in "perfect focus system" was employed for Z drift correction. Step-size between z slices was set to 0.8µm. Timelapses images were captured in increments of 15 minutes over periods of 15-40 hours. The temperature-controlled microscope imaging chamber was set at 37°C for all experiments. All samples were imaged at 50ms exposure time.

Imaging data processing

NIS Elements software was employed for the generation maximal intensity projections across all acquired Z slices. The resultant projections were utilized for all downstream analysis. Timelapses acquired in a row-wise snake formations were stitched together using the "Image stitching" plugin in ImageJ (version v1.54f) for ease of analysis. Signal intensity line profiles were obtained through ImageJ.

Imaging data analysis

For the phase duration tracing in RSV+ infected cells, in cases where RSV entry occurs in middle of an active cell cycle phase, that phase's duration is calculated from the point of infection and was only analyzed if the remaining duration was equal to or higher than half the established median duration of the corresponding phase. An infection was only considered to be in the middle of a phase if both the entry frame and the frame directly prior to entry depict the same cell cycle phase. Phase duration data was indexed based on successful phase completion and plotted in Kaplan-Meier curves to depict the cumulative probability of phase completion at a given timepoint in a time-lapse. RSV-infected cells were categorized as progressed infections when they displayed an accumulation of fluorescently labelled G proteins on their cell membranes.

Statistical analysis

GraphPad Prism 10 (GraphPad Software; San Diego, CA, USA) was utilized for figure generation and statistical analysis. Cell cycle phase distributions in infected and uninfected cells were compared using 2-way ANOVA with Dunnett's multiple comparisons test. Kaplan-Meier curves displaying cell cycle phase durations were compared using the log-rank test. Results were only considered significant with p-values <0.05.

Results

PIP-FUCCI accurately demarcates cell cycle phase transitions in A549 cells

Our initial objective was to establish the PIP-FUCCI$^{G/R}$ reporter (Grant and Kedziora 2018) (Figure 3A) in RSV-permissive A549 cells. To that end, we generated PIP-FUCCI$^{G/R}$ reporter lines, from which we isolated a single monoclone for further characterization (Figure 3B). PIP-FUCCI$^{G/R}$ generates a green fluorescent mVenus signal in cell nuclei during G1, which is rapidly degraded upon their transition into S phase. Early S phase is characterized by a lack of fluorescence in the nucleus, followed by a gradual buildup of the mCherry fluorophore after a short period. Progression into G2 phase parallels the continued accumulation of mCherry with a new wave of nuclear mVenus expression, resulting in yellow nucleus. Mitosis initiation is marked by the breakdown of the nuclear envelope and subsequent release of fluorophores into the cytosol, after which the cell splits and the cycle begins anew. For live imaging, PIP-FUCCI$^{G/R}$ nuclei were stained with Sir Hoechst to ensure accurate tracking during periods with no traceable fluorescence.

To validate the accuracy of the PIP-FUCCI system, we stained WT A549 and PIP-FUCCI$^{G/R}$ cells with DAPI to perform FACS-based DNA content analysis (Figure 3C). The variation in DNA content before and after DNA replication manifests as two peaks in a frequency histogram, with the lower DAPI peak representing cells in G1, the higher peak depicting cells undergoing G2 and M, and the bridge between the two peaks portraying cells in S phase (Figure 3C, top panel). To establish that this readout is representative of the population's cell cycle state, we induced G1 arrest in PIP-FUCCI$^{G/R}$ cells through CDK4/6 inhibitor Palbociclib. Drug treatment diminished the S and G2/M phase populations, compared to the DMSO controls. Plotting PIP-mVenus fluorescence against DNA content in PIP-FUCCI$^{G/R}$ cells displays dot plots that parallel the cell cycle phase distributions observed in the frequency histograms (Figure 3C, middle panel). Gem[1-110]-mCherry plots against DNA content displayed similar distribution patterns (Figure 3C, bottom panel). Quantifying the phase fractions in A549 cells returned a G1 population of 63.16%, along with 16.97% of S phase and 18.14% of G2 phase cells. The DMSO-treated PIP-FUCCI$^{G/R}$ samples revealed 51,98% of the population to be in G1 phase, while 39,67% and 7,42% were attributed to S and G2 phase respectively. The observed phase distributions were within the expected margins for A549 cells, confirming the efficacy of the PIP-FUCCI system as a cell cycle reporter. (Méndez-Callejas et al. 2017; Moghadamtousi et al. 2014)

Cell cycle phase distributions and durations naturally oscillate

In an effort to capture the natural variation in cell cycle phase divisions across a growing population, we recorded the phase fractions of a PIP-FUCCI$^{G/R}$ population across early (0h), mid (8.5h) and late (17h) timepoints through live time-lapse microscopy (Figure 4A). The fractions at 0h matched the distributions we observed in the DMSO-treated PIP-FUCCI$^{G/R}$ cells in Figure 3C, however at later time points we noted a reduction in the G1 population

A.

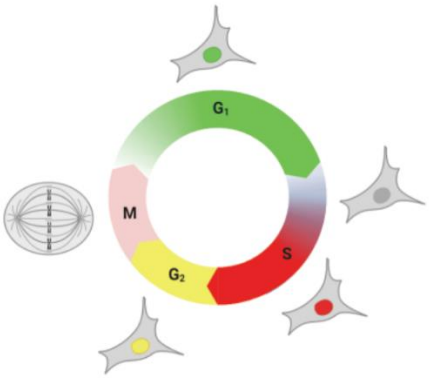
G1
S
G2
M

B.

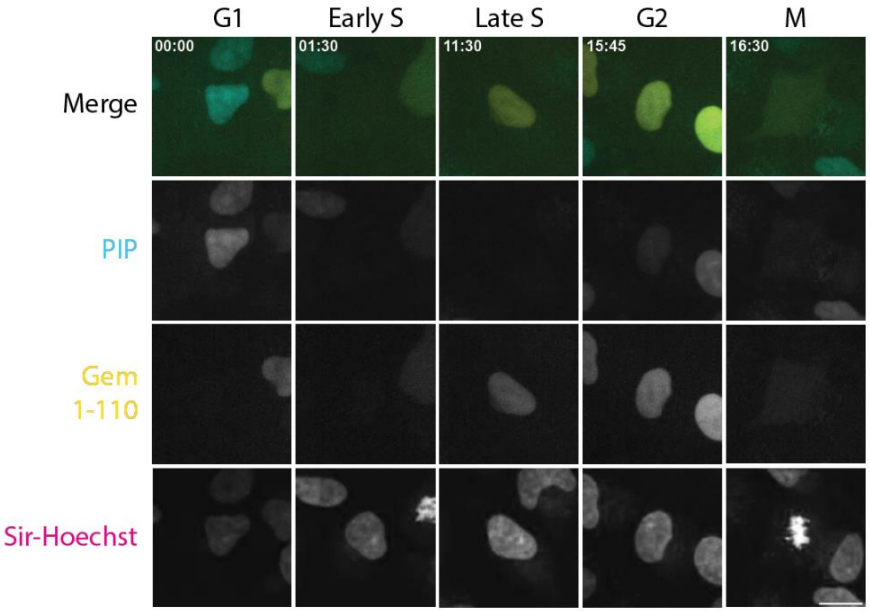
G1
Early S
Late S
G2
M
00:00
01:30
11:30
15:45
16:30
Merge
PIP
Gem
1-110
Sir-Hoechst

C.

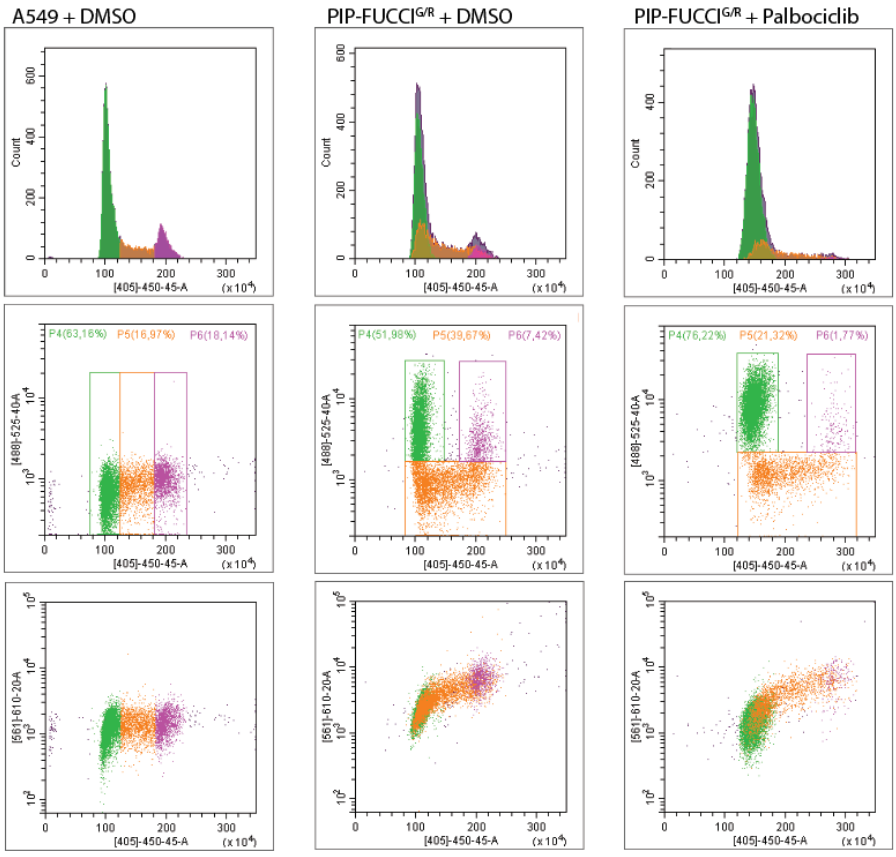
A549 + DMSO
PIP-FUCCI G/R + DMSO
PIP-FUCCI G/R + Palbociclib
Count
[405]-450-45-A
P4(63,16%) P5(16,97%) P6(18,14%)
P4(51,98%) P5(39,67%) P6(7,42%)
P4(76,22%) P5(21,32%) P6(1,77%)
[488]-525-40-A
[561]-610-20-A

Figure 3. Establishing the PIP-FUCCI system in A549 cells. (A) *A diagram depicting* PIP-FUCCI$^{G/R}$ *cell cycle labelling. Green nuclei correspond to G1 , followed by a brief period of no nuclear fluorescence denoting early S, red nuclei indicating mid-late S and yellow nuclei signifying G2. (B) Representative images of the* PIP-FUCCI$^{G/R}$ monoclone *undergoing the various cell cycle stages. Merged images depict PIP-mVenus (in cyan) and Gem[1-110]-mCherry (in yellow) expression. The time-lapse was acquired over a 17.5h period, with 15-minute intervals. 0h represents the starting point of the time-lapse. Sir-Hoechst staining was utilized to track cell nuclei during periods with no nuclear fluorescence. Scalebar = 10µm.* ***(C)*** *Histograms displaying the variation in DNA content through nuclear DAPI staining of DMSO- and Palbociclib-treated (500nM)* PIP-FUCCI$^{G/R}$ *and WT A549 cells (top panel). DAPI signal was assessed against PIP-mVenus (middle panel) and Gem[1-110]-mCherry (bottom panel) fluorescence in a dot-plot to estimate cell cycle phase fractions.*

and a subsequent increase in the S population. More specifically, at 8.5h the G1 fraction was reduced from 51.4% to 48.3%, and finally 43.4% after 17h. The S phase population growth inversely parallels the pattern of G1 fraction shrinkage. At both 8.5h and 17h, the proportion of cells undergoing mitosis seems to have doubled from the 0.9% M phase cells at 0h. The proportion of cells undergoing G2 phase remains relatively consistent across all three timepoints. The increased M phase fractions in later timepoints could indicate the cells entering a period of exponential growth. The shift between the G1 and S populations may represent the variation in cell cycle phase durations.

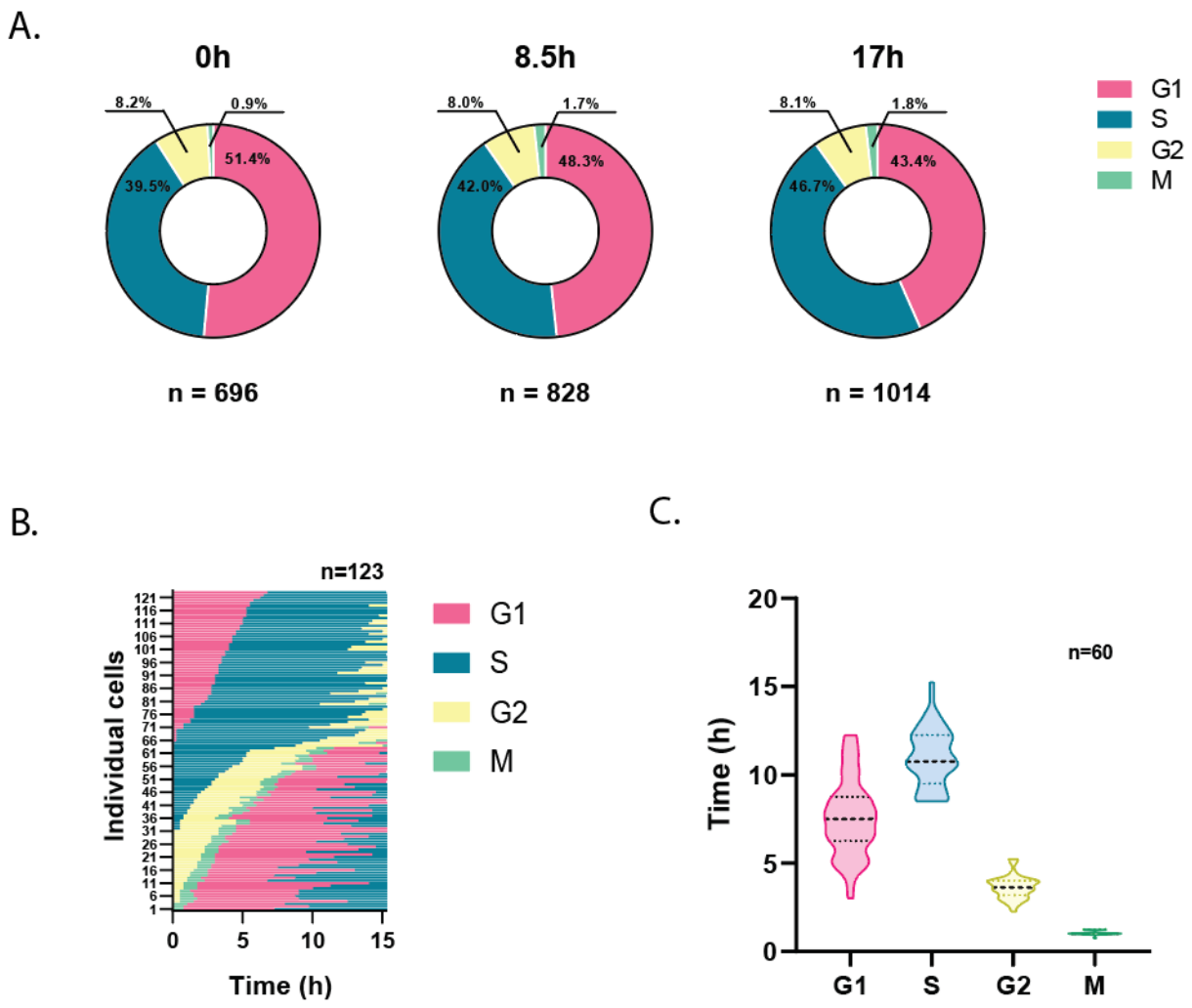

Figure 4. Characterizing the cell cycle profile of A549 cells. (A) *Pie charts depicting the fractions of cell cycle phases in* PIP-FUCCI$^{G/R}$ *cells at three different timepoints (0h, 8.5h and 17h) in a fixed field of view across a single time-lapse. n values indicate the number of cells analyzed per timepoint.* ***(B)*** *Bar graph mapping the phase lengths of individual* PIP-FUCCI$^{G/R}$ *cells across a 15.25h imaging period.* ***(C)*** *Violin plots displaying the natural variation in cell cycle stage duration. The dashed lines represent the median. The dotted lines represent the upper and lower quartiles. n values represent the total number of cells analyzed.*

To further investigate the variability in cell cycle stage durations, we tracked individual PIP-FUCCI$^{G/R}$ cells across a 17.5h period, while noting phase lengths (Figure 4B). We isolated the spans with observable start and end points throughout the timelapses, which we plotted to display the scale of natural variation in phase length (Figure 4C). On average, S appeared to be the longest stage, with a median of 10.75±1.60h, followed by G1 with a median duration of 7.5±2.14h. G2 and M spans were far more consistent, displaying median lengths of 3.63±0.64h and 1.00±0.13h respectively. G1 exhibited the greatest variability in phase durations, with the shortest observed phase being 3h and the longest extending up to 12.25h. Calculating the sum of the obtained cell cycle phase medians returns a total cell cycle median of 22.88±2.75, which matches the doubling times outlined in previous studies (Nisar et al. 2023; Sappington et al. 2016). Overall, we confirmed that the PIP-FUCCI$^{G/R}$ cell line was able to accurately delineate cell cycle phases in line with published work and determined that A549 cells display a degree of natural variation in cell cycle phase fractions and durations, especially in regards to G1 and S phases.

The P-STAb construct does not alter normal A549 cell cycling

Our next goal was to generate a novel cell line that could effectively facilitate the simultaneous visualization of cell cycle phase progression and RSV infection. We contemplated that the green cytosolic fluorescence of STAb-AausFP1 reporter in the P-STAb cell line may complicate analysis when paired with the green nuclear signal of PIP-mVenus in the PIP-FUCCI sensor. To that end, we produced a new variant of the PIP-FUCCI cell line expressing PIP-mCherry and Gem[1-110]-BFP fusion proteins (PIP-FUCCI$^{R/B}$). We sequentially transduced both of our PIP-FUCCI reporter lines with the STAb-AausFP1 and HALO-P-ST. HaloTag ligand JF646 was administered to detect cells expressing P-ST with a far-red fluorescent signal. Monoclones were selected for the newly generated P-STAb-PIP-FUCCI$^{G/R}$ and P-STAb-PIP-FUCCI$^{R/B}$ cell lines through FACS, sorting for low-medium PIP and P-ST expression to minimize the formation of fluorescent aggregates (Figure 5A). Unfortunately, due to technical difficulties we were unable to isolate serviceable P-STAb-PIP-FUCCI$^{R/B}$ monoclones. Due to time constraints, we were prompted to utilize the P-STAb-PIP-FUCCI$^{G/R}$ for all further experiments. It is important to note that the combined green fluorescent signals emitted from PIP-mVenus and STAb-AausFP1, made delineating the G1/S and S/G2 phase transitions relatively challenging. We utilized signal intensity line profiles to quantify differences in green fluorescence intensity across the nucleus and cytosol of a single P-STAb-PIP-FUCCI$^{G/R}$ cell undergoing G1, S and G2 phase (Supplementary Figure 1). We noted variations in nuclear signal intensity across all phases, albeit the intensities between the S and G2 phase nuclei were relatively small.

A.

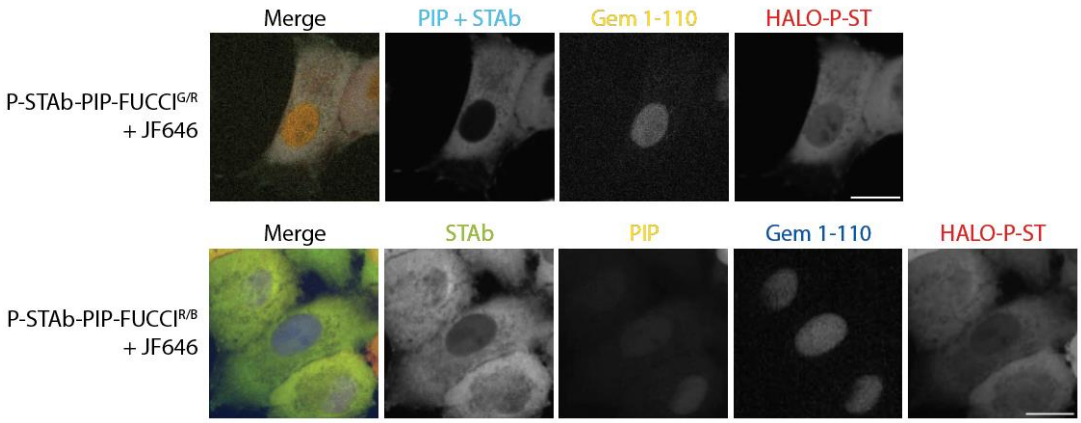
Merge
PIP + STAb
Gem 1-110
HALO-P-ST
P-STAb-PIP-FUCCI$^{G/R}$ + JF646
Merge
STAb
PIP
Gem 1-110
HALO-P-ST
P-STAb-PIP-FUCCI$^{R/B}$ + JF646

B.

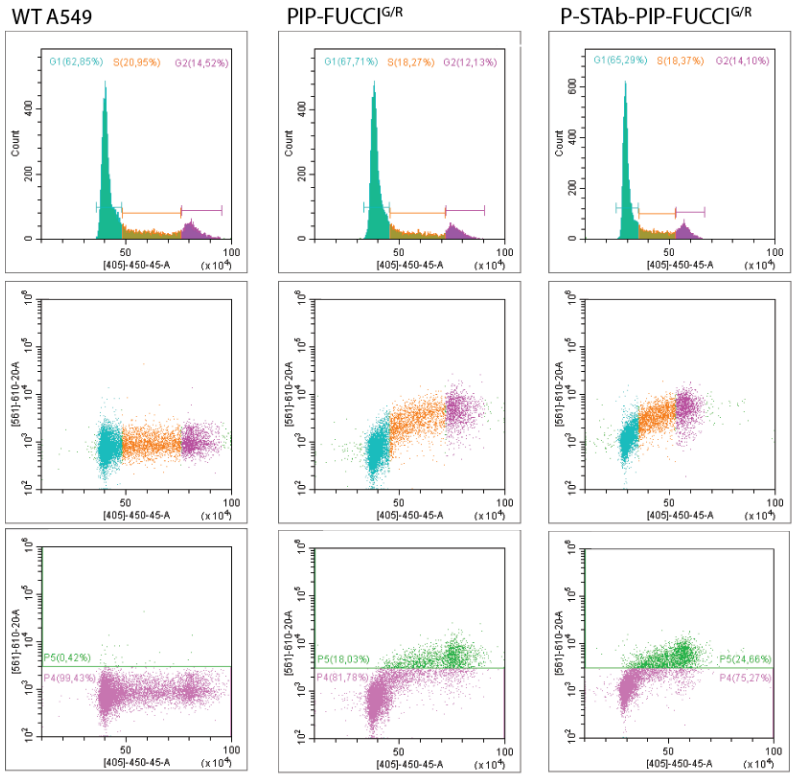
WT A549
PIP-FUCCI$^{G/R}$
P-STAb-PIP-FUCCI$^{G/R}$
G1(62,85%) S(20,95%) G2(14,52%)
G1(67,71%) S(18,27%) G2(12,13%)
G1(65,29%) S(18,37%) G2(14,10%)
Count
[405]-450-45-A
[561]-610-20-A
P5(0,42%)
P4(99,43%)
P5(18,03%)
P4(81,78%)
P5(24,66%)
P4(75,27%)

C.

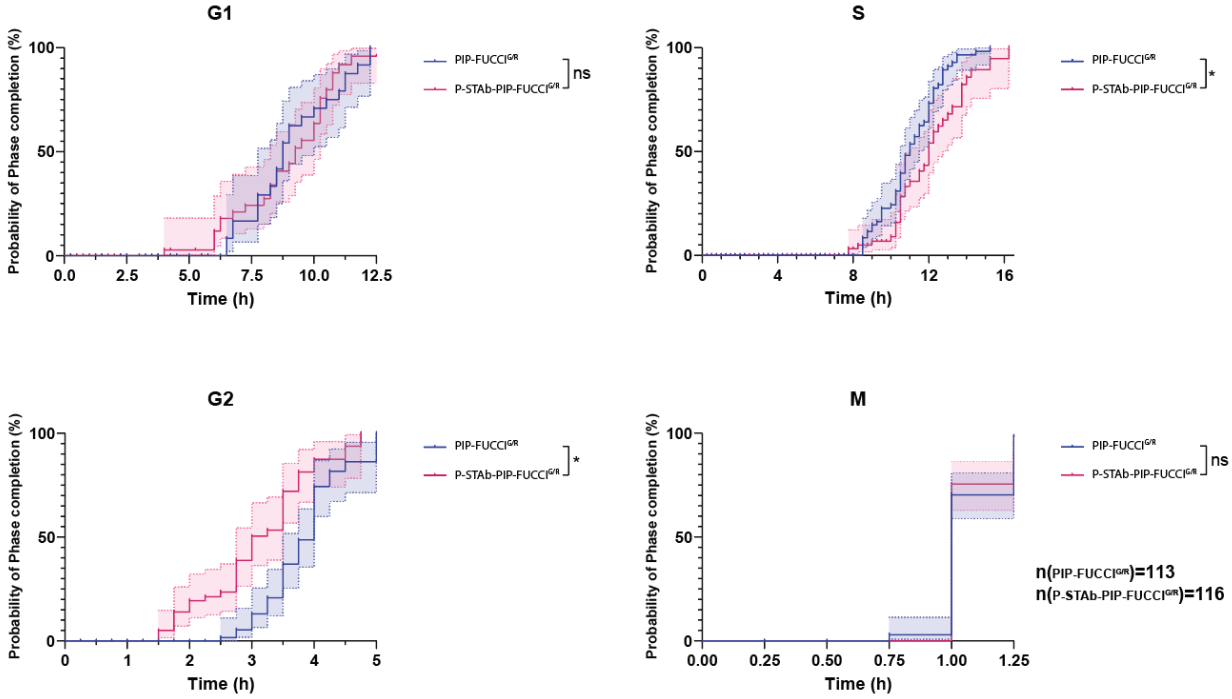
G1
S
G2
M
Probability of Phase completion (%)
Time (h)
PIP-FUCCI$^{G/R}$
P-STAb-PIP-FUCCI$^{G/R}$
ns
*
n(PIP-FUCCI$^{G/R}$)=113
n(P-STAb-PIP-FUCCI$^{G/R}$)=116

Figure 5. Validating cell lines for simultaneous tracking of RSV infection and cell cycle progression. ***(A)*** *Representative images of the* P-STAb-PIP-FUCCI$^{G/R}$ *and* P-STAb-PIP-FUCCI$^{R/B}$ *monoclones supplemented with JF646 HaloTag ligand (1:1000). Top panel merged image depicts PIP-mVenus and STAb-AausFP1 (in cyan), Gem[1-110]-mCherry (in yellow) and HALO-P-ST (in red) expression levels. Bottom panel merged image displays STAb-AausFP1 (in green), PIP-mCherry (in yellow), Gem[1-110]-BFP (in blue) and HALO-P-ST (in red) expression. Scalebars = 10µm.* ***(B)*** *Histograms matching the cell cycle phase distributions of wildtype A549,* PIP-FUCCI$^{G/R}$ *and* P-STAb-PIP-FUCCI$^{G/R}$ *cell populations through peaks generated by the changing in DNA content (top panel). Lower panel dot plots present the analogous expression of Gem[1-110]-mCherry between* PIP-FUCCI$^{G/R}$ *and* P-STAb-PIP-FUCCI$^{G/R}$ *cells in the context of DNA content.* ***(C)*** *Kaplan-meier curves comparing the observed phase durations of* PIP-FUCCI$^{G/R}$ *and* P-STAb-PIP-FUCCI$^{G/R}$ *cells. Data indexing was based on successful phase completion and plotted depicting the cumulative probability of phase completion at a given timepoint. Error bars represent SD. n values display the number of cells analyzed per cell line (*: p< 0.05)*

To confirm that P-STAb-PIP-FUCCI$^{G/R}$ cell cycle profile still matched the original PIP-FUCCI$^{G/R}$, we stained the cells with DAPI to perform DNA content analysis, utilizing WT A549 cells as a control (Figure 5B). Quantifying the cell cycle phase fractions revealed matching distributions across all three lines, within the margins of observed natural variation (Figure 5B, top panel). This is reinforced by mapping the Gem[1-110]-mCherry signal against DNA content, which returned relatively analogous plots across both PIP-FUCCI lines (Figure 5B, middle panel). Using WT A549 autofluorescence to designate the positive signal threshold, we quantified the proportions of Gem[1-110]-mCherry positive cells between the PIP-FUCCI models (Figure 5B, bottom panel). 18.03% of PIP-FUCCI$^{G/R}$ cells were positive for Gem[1-110]-mCherry, while P-STAb-PIP-FUCCI$^{G/R}$ returned a fraction of 24.66%, both of which fell within the expected margins established prior. Finally, we compared the phase duration profiles between the two cell lines through live-cell time-lapse imaging, which we presented through Kaplan-Meier curves depicting the cumulative probability of phase completion across a specific time period (Figure 5C). The graphs displayed no significant differences between G1 and M durations, however we did note significant differences in S and G2 phase durations. It seems that the average span of S phase has extended by approximately 1h in the new cell line, while G2 phase became 1h shorter. We attribute these differences to the previously mentioned lowered detection sensitivities between the PIP-mVenus and STAb-AausFP1 signals, as their overlap introduces some difficulties in identifying the early stages of G2 phase. However, since the shifts in both curves are relatively consistent, we determined that the model is suitable to use and employed it for all further experimentation.

RSV virions preferentially infect A549 cells in S phase and disfavor G1 phase

We sought to establish whether RSV virion infection rates varied depending on the cell cycle state of the target host cell at the point of infection. Infecting P-STAb-PIP-FUCCI$^{G/R}$ cells with RSV and tracking them with live-cell imaging permits us to determine the timepoints of invididual RSV infections, as well as discern the cell cycle phase of their host cells at the point of entry (Figure 6A). In an effort to ensure a fair comparison between the infected and control populations, we limited our entry tracking to a period of 6 hours post-RSV inoculation (<6hpi). Across three separate experiments, we recorded the timepoint and the corresponding cell cycle phase of each instance of RSV entry within that period, ultimately calculating the median infection time (MIT) for each experiment (Figure

6B). MIT represents the period with the highest incidence of RSV infections in a particular timelapse, which we utilized as a point of comparison for phase distributions between the infected and uninfected populations in each experimental replicate. For example, the MIT in Experiment 1 (Exp 1) was determined to be 1.5hpi. Hence, we utilized this timepoint to quantify the cell cycle phase fractions of cells in a control well (Control MIT), as well as cells that remained uninfected within the RSV+ well (RSV+ uninfected MIT).

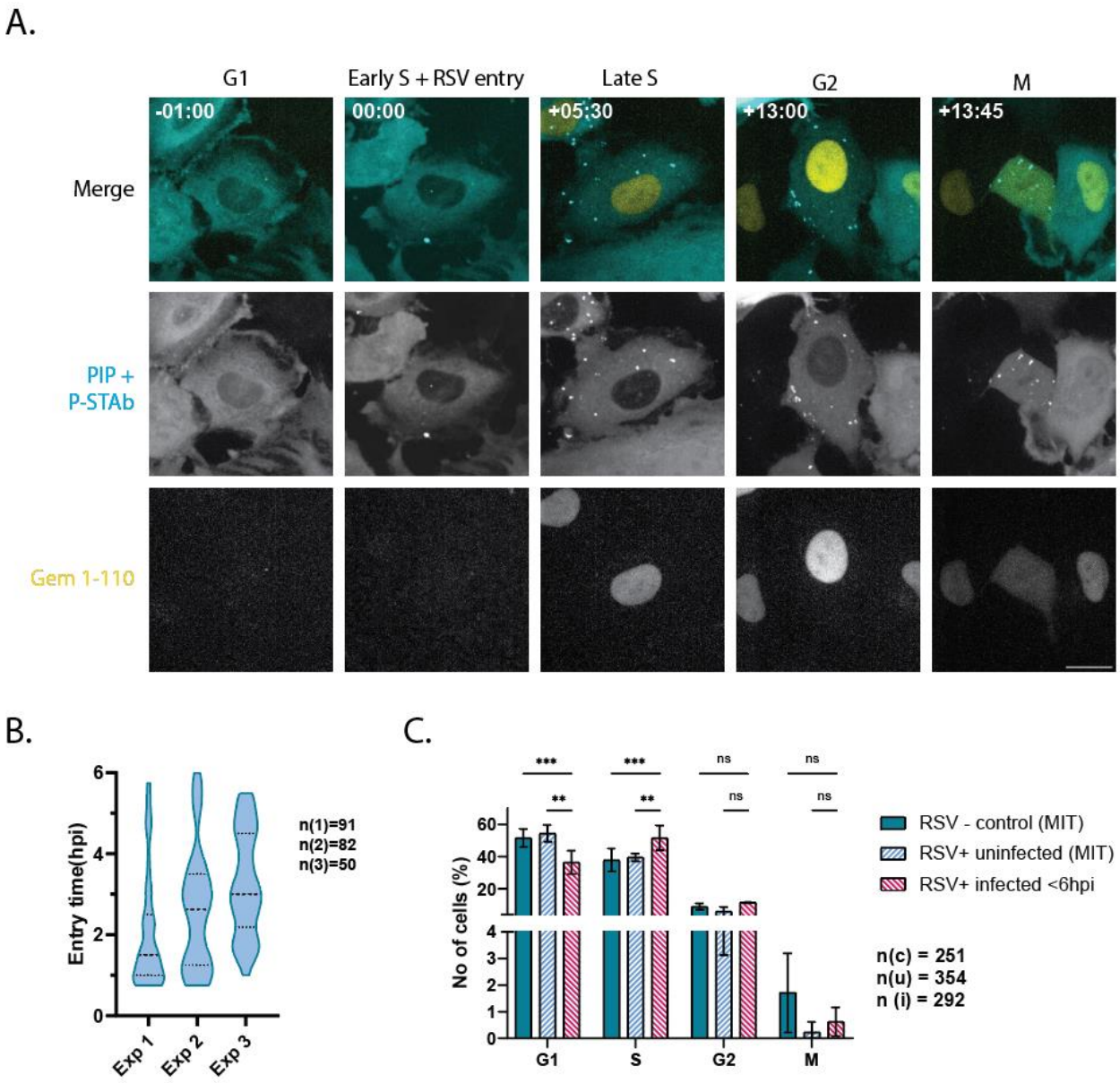

Figure 6. Examining the probability of RSV infection in various cell cycle stages. (A) *Representative images of a* P-STAb-PIP-FUCCI$^{G/R}$ *cell being infected with RSV across a long-term time-lapse. Merged images depict PIP-mVenus (in cyan) and Gem[1-110]-mCherry (in yellow). RSV entry occurs in the early S stage. Timepoints are depicted relative to the frame of RSV entry. Scalebar = 10µm.* ***(B)*** *Violin plots outlining the distribution of RSV entry times within the first 6 hours of RSV application (<6hpi) across Experiments 1 (MOI=0.63), 2 (MOI = 0.45) and 3 (MOI=0.37). The dashed line represents the median infection time (MIT) for each experiment. The dotted lines correspond to the upper and lower quartiles for each plot.* ***(C)*** *Bar graph comparing cell cycle phase proportions between cells in an RSV- control well (RSV- control) and uninfected cells in the RSV+ well (RSV+ uninfected) at experiment-specific MITs, as well as RSV+ infected cells at the points of viral entry (RSV+ infected <6hpi). The displayed results represent the mean±SD of distinct biological replicates (n=3). Displayed n values denote the total number of cells analyzed per condition. (** : p<0.01) (*** : p<0.001)*

It is important to note that samples were seeded into their corresponding wells simultaneously to maintain a degree of synchronicity. With the phase distribution across the differing populations established, their interrelation may be examined. Combining the readouts from all three experiments, we identified significantly higher proportions of S phase in newly infected cells, in comparison to the uninfected and control populations (Figure 6C). These findings suggest that RSV preferentially infects A549 cells undergoing S phase, while significantly disfavoring infecting cells in G1 phase. We did not observe any notable patterns correlating incidence of RSV infection with G2 or M phase cells. A comparison between the cell cycle stage fractions of the control well and total infected well populations revealed matching proportions across all phases, further validating our results (Supplementary Figure 2). Together, these findings indicate that host cell cycle affects the probability of RSV entry.

RSV infection extends the duration of G1 and M in A549 cells

We wanted to assess whether cell cycle phase durations are altered in RSV-infected cells and to determine whether the uninfected cells in the well exposed to the virus inoculum displayed altered cycling behaviors. We tracked the phase spans of infected cells (RSV+ infected <6hpi) and RSV+ uninfected cells (Figure 7A) through long-term (15.25h - 28h) imaging of P-STAb-PIP-FUCCI$^{G/R}$ lines and compared them to an RSV- control population. While the S and G2 cell cycle phase durations remained relatively unaltered across all conditions, the G1 phase duration appeared to be severely extended in RSV-infected cells. As expected, some of cells that were infected in G1 remained in G1 for up to 28 hours, confirming previous observations of RSV infection inducing G1 arrest (Bakre et al. 2015; Bian et al. 2012; Laiho et al. 1990). However, it is important to note that some of the cells that entered prolonged G1 phases lasting between 15-27.25h were still able to transition into S phase, suggesting that infection may elongate G1 in some cells without inducing outright arrest. Interestingly, the introduction of RSV also seemed to significantly extend the duration of G1 in the RSV+ uninfected population by an average of 1-2 hours. This effect may denote some possible RSV-induced extracellular signaling that could affect the cycling of uninfected cells in the RSV+ well. Finally, we discovered that RSV disrupted the progression of mitosis in approximately 17.28% of infected cells (Supplementary Figure 3), extending the duration of mitosis up to 2.5 hours. Further inspection revealed that the disruption generally stems from a delay in the metaphase/anaphase, where chromosomes align at the center of the cell along the metaphase plate and split into sister chromatids. From this point, control cells generally require less than 15 minutes to enter telophase and split into daughter cells, while the prolonged M cells tend to get stuck in the metaphase/anaphase a longer period and struggle to transition into telophase (Figure 7C). In summary, our results demonstrate that active RSV infection can elongate the G1 and M phase durations of A549 cells, without inducing permanent arrest.

A.

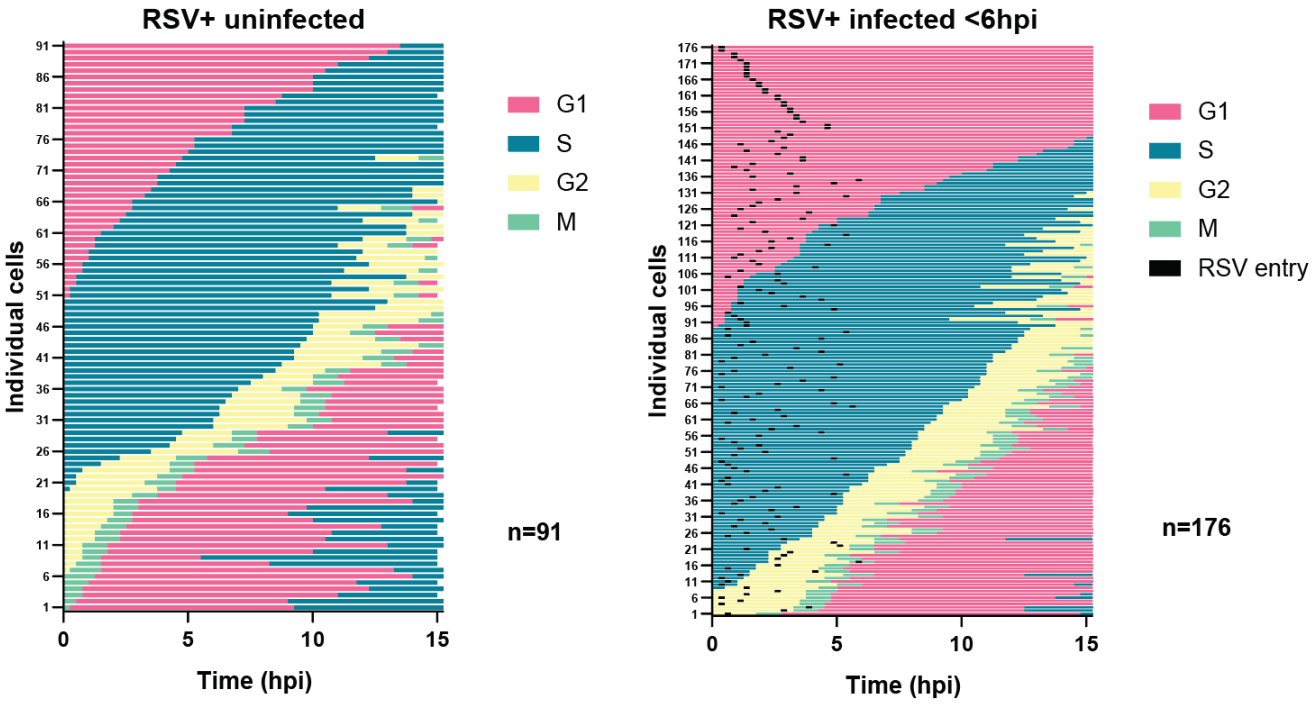
RSV+ uninfected
Individual cells
Time (hpi)
G1
S
G2
M
n=91
RSV+ infected <6hpi
Individual cells
Time (hpi)
G1
S
G2
M
RSV entry
n=176

B.

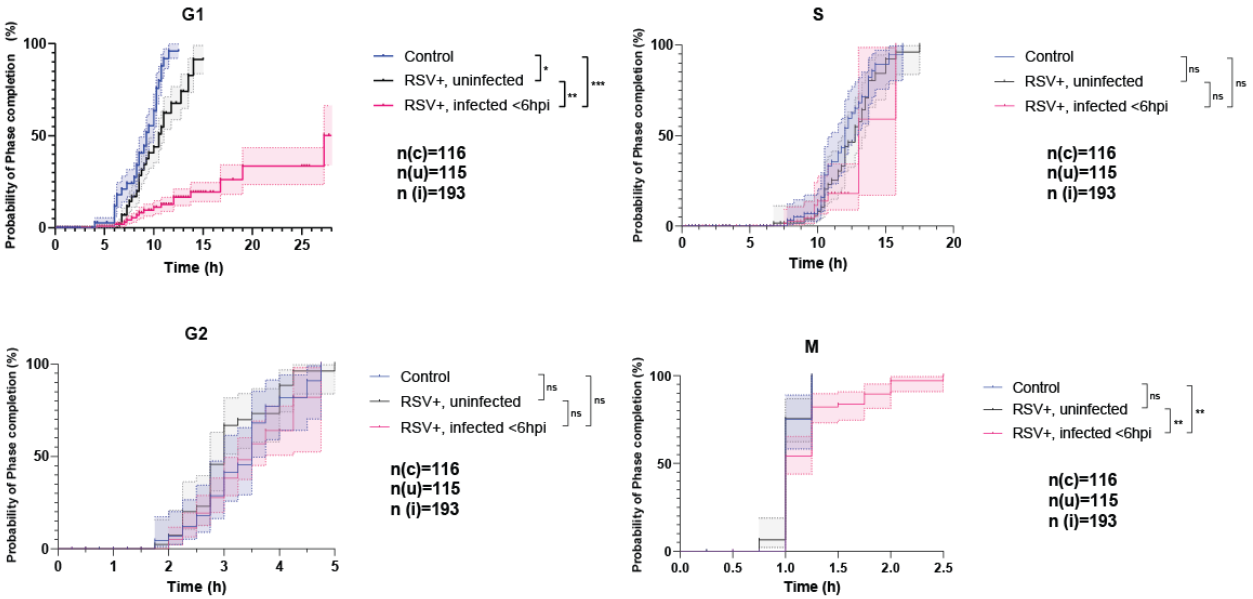
G1
Probability of Phase completion (%)
Time (h)
Control
RSV+, uninfected
RSV+, infected <6hpi
n(c)=116
n(u)=115
n (i)=193
S
Probability of Phase completion (%)
Time (h)
Control
RSV+, uninfected
RSV+, infected <6hpi
n(c)=116
n(u)=115
n (i)=193
G2
Probability of Phase completion (%)
Time (h)
Control
RSV+, uninfected
RSV+, infected <6hpi
n(c)=116
n(u)=115
n (i)=193
M
Probability of Phase completion (%)
Time (h)
Control
RSV+, uninfected
RSV+, infected <6hpi
n(c)=116
n(u)=115
n (i)=193

C.

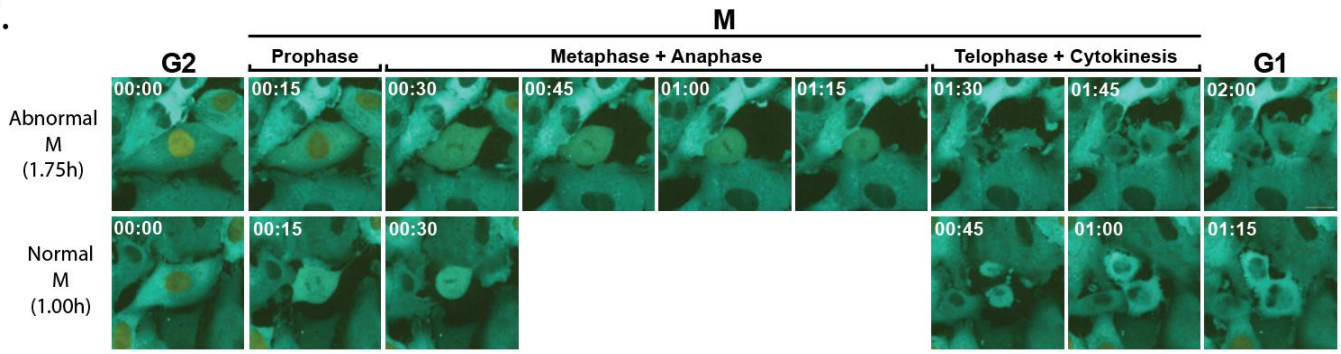
M
G2
Prophase
Metaphase + Anaphase
Telophase + Cytokinesis
G1
Abnormal M (1.75h)
Normal M (1.00h)
00:00
00:15
00:30
00:45
01:00
01:15
01:30
01:45
02:00

Figure 7. Investigating the effects of RSV infection on cell cycle phase durations. (A) *Bar graphs depicting the phase durations of individual infected and uninfected cell populations grown within an RSV+ well. The black dashes in the RSV+ infected graph represent points of viral entry. n values represent the number of cells analyzed per condition.* ***(B)*** *Kaplan-Meier curves outlining the alterations in cell cycle stage lengths across RSV+ infected, RSV+ uninfected and control populations. Only cells infected in the first 6h of imaging were incorporated into the RSV+ infected population. The results represent the values from distinct biological replicates (n=3). The displayed n values represent the number of cells analyzed per corresponding condition. Error bars represent SD. (* : p<0.05) (** : p<0.01)(*** : p<0.001)* ***(C)*** *Representative images of an RSV-infected cell undergoing a prolonged metaphase and anaphase, compared to a normally cycling cell. Scalebar = 10μm.*

Progressing RSV infections are characterized by an elongated G1 and S phase

To investigate the interrelation of RSV infection and host cell cycle state in the context of successfully progressing infections, we employed a fluorescently labelled antibody specific for the viral G protein. Administering the antibody along with the viral inoculum permits the identification of cells with progressed RSV infections, as they will begin to accumulate newly synthesized viral G proteins at their outer cell membranes, which we can trace through live-cell fluorescent imaging (Figure 8A). This allows us to retrospectively examine the earlier stages of progressed infections and elucidate the factors that contribute to their manifestation. For example, in order to assess whether RSV entry in a particular phase of the cell cycle affected infection progression, we compared the phase fractions between progressing and non-progressing cells at the points of viral entry (Figure 8B). Our findings did not indicate any cell cycle-dependent preferential entry for RSV virions that go on to generate progressed infections. We then analyzed the variation in phase durations between progressing and non-progressing populations (Figure 8C). The comparison did not yield any significant findings relating to G2 and M phases, however, we did note a significant lengthening of the average G1 and S phases in progressing infections, when compared to their non-progressing counterparts. These elongations could be illustrating a correlation between infection progression success and replication stress. To summarize, our results did not unveil a pattern between cell cycle phase-dependent RSV entry and infection progression probability, however cells with actively progressing RSV infections displayed longer average G1 and S phases, possibly due to increased replication stress.

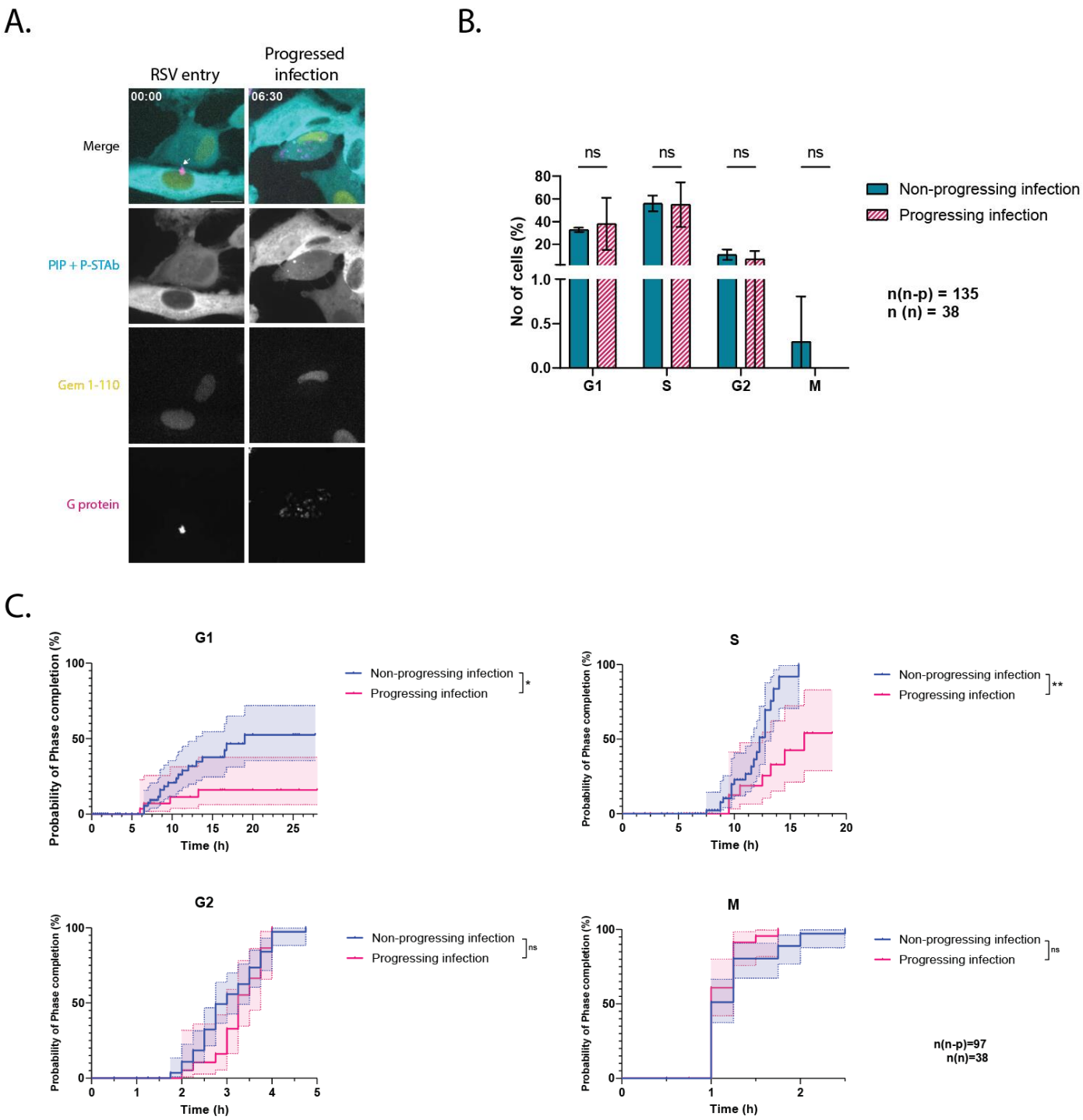

Figure 8. Examining the interrelation between cell cycle and RSV infection progression. (A) *Representative images of fluorescently labelled G antibodies binding to G proteins accumulating on the host cell membrane at the onset of RSV infection progression. Merged images depict PIP-mVenus and P-STAb-AausFP1 (in green), Gem[1-110]-mCherry (in red) and viral G protein (in magenta). Invading vRNP is marked by white arrowhead. Time points are displayed relative to the time of RSV entry. Scalebar = 10µm.* ***(B)*** *Bar graph displaying the cell cycle phase distributions of cell populations with progressing and non-progressing RSV infections at the point of viral entry. RSV entry had to occur within the first 6 hours of infection to be included in the analysis. The outlined results represent the mean±SD of distinct biological replicates (n=3). Displayed n values depict the number of cells analyzed per condition.* ***(C)*** *Kaplan-Meier curves illustrating differences in phase durations between* P-STAb-PIP-FUCCI$^{G/R}$ *populations with progressed and non-progressed RSV infections. All analyzed cells incurred RSV entry at <6hpi. Results illustrate the values obtained from separate biological replicates (n=3). Displayed n values depict the number of cells analyzed per condition. Error bars represent SD. (** : p<0.01)*

Discussion

Our study was the first to investigate the interrelation between the early stages of RSV infection and host cell cycle state. The P-STAb system allows for the clear visualization of viral entry and subsequent vRNA replication. The application of fluorescently labelled viral G protein antibodies seamlessly permits the identification of progressing infections. Combining P-STAb with PIP-FUCCI reporters, we were able to obtain novel insights into the field, while prompting compelling follow-up questions.

Our results indicated that RSV virions preferentially infect cells undergoing S phase and are significantly less inclined to infect cells in G1 (Figure 6C). This pattern cannot be attributed to differences in cellular surface area, as most cells tend to reach their maximal size in G2 phase, which displayed no preferential RSV entry. These differences in infection rates are most likely prompted by cell cycle-dependent changes in the host surface receptor repertoire. Studies have established HSPGs as the primary receptors for RSV entry in A549 cells due to their aberrant overexpression in the model line (Feng, Xu, and Xie 2022; Hallak, Spillmann, et al. 2000; Pruessmeyer et al. 2010). Unfortunately, not much is known about the dynamics of HSPGs in A549 cells or their effects on cell cycle progression. Syndecan-1 (SDC-1), a major member of the HSPG group, was shown to modulate the epithelial-mesenchymal transition (EMT) of A549 cells by translocating to the nucleus (Kumar-Singh et al. 2021). A study on rat hepatoma cells correlated G1 phase with an increased concentrations of nuclear HSPGs and noted a reduction in nuclear HSPGs following the G1/S transition (Fedarko, Ishihara, and Conrad 1989), possibly paralleling the patterns of phase-dependent preferential RSV infection we observed in A549 cells. To elucidate HSPG dynamics in relation to the cell cycle, we suggest performing immunofluorescence staining for SDC-1 in PIP-FUCCI cells, after which the surface expression of the receptor at various cell cycle phases can be quantified through flow cytometry.

EGFR is well known for modulating cytoplasmic signaling cascades, initiated through the binding of its epidermal growth factor (EGF) ligand. Besides that, EGF binding can also induce EGFR nuclear translocation, which shuttles the receptor to the inner nuclear membrane or directly into the nucleoplasm (Cao et al. 1996; Kamio et al. 1990; Rodrigues et al. 2016). The rate of EGFR internalization was found to be increased in a variety of cancers, as well as some cancer cell lines, including A549 cells (Bazzani et al. 2017; Psyrri et al. 2005; Shen et al. 2022). Although EGFR does not possess a DNA binding domain, it can interact with DNA-binding transcription factor E2F1 and signal transducer and activator of transcription 3 (STAT3) to modulate gene expression (Hanada et al., 2006; Lo et al., 2005). Acting as a transcriptional coactivator, EGFR was shown to upregulate the expression of cyclin D1, suggesting that nuclear EGFR can aid the initiation of G1(Lin et al. 2001). Additionally, the EGFR/E2F1 complex is involved in the activation of cell cycle regulator B-Myb in late G1, which in turn promotes the cell's transition into S phase (Hanada et al. 2006; Joaquin and Watson 2003). With that in mind, the continuous nuclear translocation of EGFR throughout G1 to stimulate cell cycle progression may explain the reduced incidence RSV entry we observed in G1 cells. However, EGFR expression is known to be highly upregulated in A549 cells (Nicholson, Gee, and Harper 2001; Zhou et al. 2018), calling the impact of EGFR internalization on RSV entry into question. A study investigating WT A549 cells found that EGF treatment caused a substantial proportion (>60%) of EGFR receptors

to colocalize with early endosome marker Rab11, supporting our theory that EGFR endocytosis may affect RSV infection rates in G1 cells.

Relating to S phase, NCL, CX3CR1 and IGF1R were all shown to be pivotal for maintaining stable DNA replication and mitigating replication stress. NCL functions as a histone chaperone and DNA helicase, thereby its involvement in facilitating DNA replication. However, it also plays a role in aiding the repair of DNA double-strand breaks (DSB) by disrupting affected nucleosomes and stalling DNA synthesis, clearing the space for the recruitment of repair proteins (Goldstein et al. 2013; Kobayashi et al. 2012). CX3CR1 promotes the repair of interstrand DNA crosslinks during S phase by recruiting FANCD2 to stalled replication forks and inducing the Fanconi anemia repair pathway (Lehto et al. 2021). Finally, IGF1R can complex with proliferating cell nuclear antigen (PCNA) to activate DNA damage tolerance (DDT) pathways that help bypass replication fork stalling and prevent fork breakage(Yang et al. 2020). IGF1R was also shown to be involved in the repair of DSBs through homologous recombination (HR) and non-homologous end joining (NHEJ) (Chitnis et al. 2014; Turney et al. 2012). However, in order to perform all of these functions the receptors have to be translocated to the nucleus during S phase, thereby potentially reducing the quantity of receptors localized at the cell membrane and conflicting with our observations of RSV virions preferentially infecting S phase cells. This discrepancy may be explained by the fact that similarly to EGFR, all three of these receptors were shown to be overexpressed in A549 cells (Gong et al. 2009; Huang et al. 2019; W. Liu et al. 2019), meaning that their intracellular concentrations may be negligible when compared to their cell membrane concentrations. Unfortunately, not much is known about the cell cycle-dependent internalization rates of NCL, CX3CR1 and IGF1R in A549 cells. Considering this, it may be advantageous to additionally validate our phase-dependent preferential RSV entry findings to confirm that the patterns we observed were accurate. A relatively simple approach to achieve that would involve arresting distinct cell populations at various cell cycle stages and infecting them with equal concentrations of RSV, in order to track entry rates across consistent populations.

Although it is known that HSPGs are the dominant RSV receptors in A549 cells, the exact proportions of RSV entry attributed to each RSV receptor have not been elucidated. To address this, we could perturb P-STAb-PIP-FUCCI$^{G/R}$ cells with selective RSV receptor inhibitors and track their effects on RSV entry rates. For example, treating cells with EGFR-specific monoclonal antibody cetuximab inhibit the EGF-dependent activation and internalization of the EGFR receptor prior to RSV inoculation (Xiong et al. 2004). The resultant alterations in phase-dependent RSV infection incidence would demonstrate the receptor's contributions to facilitating RSV entry in relation to host cell cycle state. We can further expand upon this, by applying a similar treatment strategy to the other RSV receptors discussed in this study and obtaining a general outline of receptor-modulated RSV entry dynamics (Bertrand et al. 2006; Ikeda et al. 2009; Low et al. 2020; Palmieri et al. 2015).

Elucidating the dynamics of RSV entry may further our understanding of RSV infection patterns. Researchers deduced that the viral G protein is not essential for successful infection of immortalized A549 and HEp-2 cells, although it is strongly beneficial (Arnold et al. 2004; Karron et al. 1997; Teng and Collins 1998). These findings suggest that, at least in cultured cells, viral F proteins are able to carry out cell attachment and membrane fusion on their own. Considering this, it could be beneficial to further dissect the processes of attachment and fusion. We suggest employing real-time 3D single particle tracking (RT-3D-SPT) technology to monitor single RSV virion interactions with cell surface receptors. RT-3D-SPT utilizes active feedback to continuously track freely diffusing

particles in 3 dimensions over a specified axial range (Hou, Johnson, and Welsher 2019). RT-3D-SPT has previously been utilized to investigate interactions between vesicular stomatitis virus (VSV) G proteins and the host cell membrane (Hou and Welsher 2019; C. Johnson et al. 2022). We could apply RT-3D-SPT to track the co-localization of viral G proteins with host receptors, potentially gaining insights into the binding rates and kinetics across the various RSV-associated receptors. Furthermore, introducing the PIP-FUCCI reporter would allow the delineation of these patterns in a cell cycle context.

Our examination of cell cycle phase durations in RSV-infected cells highlighted an elongation of G1 phase which exceeded the range of general A549 phase length heterogeneity we established in Figure 4A. This goes in line with the cases of RSV-induced G1 arrest reported in previous studies (Bakre et al. 2015; Bian et al. 2012). Although the majority of RSV-infected cells that enter a prolonged G1 phase are likely to insinuate arrest, we have observed cells with abnormally elongated G1 phases that ultimately transitioned into S phase (Figure 7B). On the other hand, our findings demonstrated that once any cell with a confirmed progressing RSV infection entered a prolonged G1 phase, they remained stuck in G1 for the remainder of the time-lapse. This could suggest that infection progression is not necessary for the induction of G1 arrest but may be required for its continued maintenance. Furthermore, we found that in cells with progressed RSV infections approximately 81.8% of G1 phase durations were prolonged, while only 50% of non-progressing infections displayed prolonged G1 (data not shown). Perhaps throughout the mechanisms that RSV can employ to induce G1 arrest (Bakre et al. 2015; Bian et al. 2012; Laiho et al. 1990), the pathways associated with progressing RSV infections are more efficacious. We could explore this pattern further, for instance by inducing RNA interference (RNAi)-based knockdowns of P53 and TGF-β in P-STAb-PIP-FUCCI$^{G/R}$ cells, in order to mitigate RSV-induced G1 arrest. Through this, we could not only determine whether one of the arrest pathways is dominant, but also elucidate whether the rates of RSV infection progression are affected by reduced G1 arrest.

In the framework of progressed infection, the cell cycle phase upon RSV entry did not seem to impact the probability of progression (Figure 8B). The significant elongation of both G1 and S phases in progressed infections directed us to consider a connection between infection progression and replication stress (Figure 8C). RSV infection was shown to induce the production of reactive oxygen species (ROS) e.g. superoxide and hydrogen peroxide (H2O2), highly reactive free radicals and known promoters of DNA damage (Casola et al. 2001). The virus incites an imbalance between the production of ROS and their attenuating antioxidants, leading to a drastic overproduction of ROS that emanate from the mitochondria (Hosakote et al. 2009; Martínez et al. 2016). The mitochondrial ROS are mediators of DSBs, as well as other of DNA lesions, ultimately enhancing oxidative stress to the point of disrupting normal cell cycling (Martínez et al. 2016; Salehi et al. 2018). Researchers have implicated ROS overproduction in inducing G1 arrest and DNA replication slowdown, which can ultimately lead to replication fork stalling (Andrs et al. 2023; Tai et al. 2020). These outcomes parallel the cell cycle disruptions we observed in cells with progressed RSV infections, potentially pointing towards a correlation between oxidative stress and infection progression success. It would be pertinent to examine this correlation further, perhaps through the use of oxidative stress indicators. Dihydroethidium and mitochondrial superoxide indicator (MitoSOX) are fluorogenic probes that could be used to detect intracellular superoxide in cells with progressing and non-progressing RSV infections, although they should only be utilized for qualitative analysis (Zielonka and Kalyanaraman 2010;

Zielonka, Vasquez-Vivar, and Kalyanaraman 2008). Intracellular H2O2 levels can be similarly tracked through the use of redox-sensitive fluorescent probes coupled to H2O2-specific peroxiredoxins (Morgan et al. 2016). Methods for the accurate quantification of intracellular ROS in live cells are currently limited. Additionally, the buildup of oxidative stress in infected cells may have resulted in the extracellular release of ROS, and its subsequent accumulation in the culture medium, which may be responsible for the minor yet significant elongation of G1 in RSV+ uninfected cells (Uy, McGlashan, and Shaikh 2011).

RSV-induced ROS production may also explain the prolonged mitosis we observed in a portion of RSV-infected cells (Figures 7B, 8C; Supplementary Figure 3). A study employing HeLa cells demonstrated that exposure to ROS disturbs spindle formation and induces a mitotic delay (G. F. Wang et al. 2017), matching the metaphase pause we observed in our samples. That being said, it would be beneficial to capture the mitotic delay in cells with DNA staining e.g. Sir-Hoechst, to more confidently establish the affected stages.

Our surveillance of non-progressing RSV-infected cells undergoing mitosis seemed to display a random distribution of vRNPs across the resultant daughter cells. In some cases, all of the invading vRNPs would be passed on to a single daughter cell, which could go on to develop a progressed infection while the other daughter cell escaped infection. If both daughter cells received vRNPs, either or both of them had a chance to develope progressed infections in seemingly varied time scales. However, once active vRNA replication was observed in cells, any subsequent mitosis generally resulted in two highly infected daughter cells. Interestingly, a pair of daughter cells with progressing infections often displayed strictly concurrent accumulations of G proteins on their cell membranes, even multiple hours after the end of mitosis. Contemplating the nature of these events, we theorize that the rate of vRNA replication is directly proportional to the rate of infection progression. Hence, even if a progressing cell were to split, as long as vRNPs are generated at the same rate in the two daughter cells they will develop progressed infections in parallel. To make any solid conclusions, we would need to acquire further examples of this phenomenon.

The largest limitation imposed on our study is related to the biological relevance of our utilized model. A549 is an immortalized cancer model with several mutations that majorly alter its cell cycling e.g. an activating KRAS mutation (Yoon et al. 2010), rendering it hardly representative of primary human epithelial cells. Additionally, A549s are also known to be prone to multinucleation and the formation of giant cells (Travaglione et al. 2006), which interfere with analysis. With all of that in mind, we selected this model to search for unprecedented connections between RSV infection and cell cycle. This pursuit required the development of complex visualization tools that, for our purposes, could only be established in A549 cells. Employing these tools, we uncovered novel findings linking the two processes together, which can now be explored in a more biologically relevant RSV-permissive model e.g. PHBE cells. To reiterate, numerous studies demonstrated that the expression and localization of RSV-associated receptors in A549 cells varies significantly from primary human epithelial cells, with many of them, especially HSPGs, being strongly overexpressed in A549 cells (Gong et al. 2009; Huang et al. 2019; W. Liu et al. 2019; Zhou et al. 2018). In fact, *in vivo* studies determined that CX3CR1 is far more likely to contribute to RSV infection in the airway epithelium than HSPGs (Green et al. 2021; S. M. Johnson et al. 2015). Thus, our observed paradigm of cell cycle phase-dependent preferential RSV entry might not be relevant to the PHBE model. However, it would be pertinent to explore the correlation of RSV infection progression with the

incidence of G1 arrest in PHBE cells, perhaps through a combination of fluorescently labelled viral G proteins and the RNAi-induced knockdowns of P53 and TGF-β, as discussed prior.

Prior to committing to major experiments, we opted to characterize the intrinsic cell cycle heterogeneity of our utilized cell line, however we have not considered the heterogeneity inherent in the infecting virion. Our group discovered that a single RSV virion can contain several vRNAs, with their numbers possibly altering the process of infection progression. It may be beneficial to categorize individual infections by the number of invading vRNAs and unearth any patterns that are concealed by virion heterogeneity. Our group is currently in the process of employing specialized visualization tools to elucidate the heterogeneity in invading vRNPs and its impact on infection progression. Furthermore, throughout this study we did not track the formation of IBs in infected cells, despite their utmost importance in the viral life cycle. IB formation marks the start of active vRNA replication and the earliest point of no return for progressing infections. Determining whether host cell cycle state has an effect on this event could broaden our understanding of the late stage RSV infection paradigm. Our group possesses the tools for the identification of inclusion bodies, which could be paired with PIP-FUCCI in future experimentation to potentially yield valuable results in the context of our study. Finally, investigating the interrelation of host cell cycle and RSV antiviral response, specifically the induction of IFN-I, could reveal novel parameters that define the variability in viral immune evasion and the innate immune response.

In conclusion, our group developed tools that permit the visualization of the intracellular stages of the RSV life cycle, which we combined with the PIP-FUCCI cell cycle reporter to investigate virus entry and infection progression against through the scope of cell cycle dynamics. Employing this combinatorial approach, we established the possibility of preferential RSV entry in S phase cells and illustrated the RSV-induced elongation of G1 and M phase durations. Examination of cell cycling patterns in progressed RSV infections revealed further lengthening of G1 and S spans, prompting theories correlating the potency of RSV infection to concomitant accumulation of oxidative stress.

References

Andrs, Martin et al. 2023. “Excessive Reactive Oxygen Species Induce Transcription-Dependent Replication Stress.” *Nature Communications* 14(1791): 1–15.

Arnold, Ralf, Brigitte König, Hermann Werchau, and Wolfgang König. 2004. “Respiratory Syncytial Virus Deficient in Soluble G Protein Induced an Increased Proinflammatory Response in Human Lung Epithelial Cells.” *Virology* 330(2): 384–97.

Bächi, Thomas, and Calderon Howe. 1973. “Morphogenesis and Ultrastructure of Respiratory Syncytial Virus.” *Journal of Virology* 12(5): 1173–80.

Bagga, Sumedha, and Michael J. Bouchard. 2014. 1170 Cell Cycle Control *Cell Cycle Regulation During Viral Infection*.

Bakre, Abhijeet et al. 2015. “Human Respiratory Syncytial Virus Non-Structural Protein NS1 Modifies MiR-24 Expression via Transforming Growth Factor-Beta.” *Journal of General Virology* 96: 3179–91.

Barr, John N., and Gail W. Wertz. 2001. “Polymerase Slippage at Vesicular Stomatitis Virus Gene Junctions To Generate Poly(A) Is Regulated by the Upstream 3'-AUAC-5' Tetranucleotide: Implications for the Mechanism of Transcription Termination.” *Journal of Virology* 75(15): 6901–13.

Bazzani, Lorenzo et al. 2017. “PGE2/EP3/SRC Signaling Induces EGFR Nuclear Translocation and Growth through EGFR Ligands Release in Lung Adenocarcinoma Cells.” *Oncotarget* 8(19): 31270–87.

Berman, Stephen. 1991. “Epidemiology of Acute Respiratory Infections in Children of Developing Countries.” *Reviews of Infectious Diseases* 13(Suppl 6): S454–62.

Bermingham, Alison, and Peter L. Collins. 1999. “The M2-2 Protein of Human Respiratory Syncytial Virus Is a Regulatory Factor Involved in the Balance between RNA Replication and Transcription.” *Proceedings of the National Academy of Sciences of the United States of America* 96(20): 11259–64.

Bertrand, F. E. et al. 2006. “Synergy between an IGF-1R Antibody and Raf/MEK/ERK and PI3K/Akt/MTOR Pathway Inhibitors in Suppressing IGF-1R-Mediated Growth in Hematopoietic Cells.” *Leukemia* 20(7): 1254–60.

Bian, Tao, John D. Gibbs, Claes Örvell, and Farhad Imani. 2012. “Respiratory Syncytial Virus Matrix Protein Induces Lung Epithelial Cell Cycle Arrest through a P53 Dependent Pathway.” *PLoS ONE* 7(5): 1–9.

Bitko, Vira et al. 2007. “Nonstructural Proteins of Respiratory Syncytial Virus Suppress Premature Apoptosis by an NF-KB-Dependent, Interferon-Independent Mechanism and Facilitate Virus Growth.” *Journal of Virology* 81(4): 1786–95.

Boersma, Sanne. 2022. “Dynamics and Heterogeneity of MRNA Translation and RNA Virus Infections.” Utrecht University. https://www.publicatie-online.nl/uploaded/flipbook/156772-Sanne-Boersma/%0Ahttps://dspace.library.uu.nl/handle/1874/416544.

Bourgo, Ryan J., Wesley A. Braden, Susanne I. Wells, and Erik S. Knudsen. 2009. “Activation of the Retinoblastoma Tumor Suppressor Mediates Cell Cycle Inhibition and Cell Death in Specific Cervical Cancer Cell Lines.” *Molecular Carcinogenesis* 48(1): 45–55.

Cao, H., Z. M. Lei, L. Bian, and Ch. V. Rao. 1996. “Functional Nuclear Epidermal Growth Factor Receptors in Human Choriocarcinoma JEG-3 Cells and Normal Human Placenta.” *Endocrinology* 136(7): 3163–72.

Carrico, Justin et al. 2023. “The Annual Economic Burden of Respiratory Syncytial Virus in Adults in the United States.” *The Journal of Infectious Diseases*: 1–12.

Casola, Antonella et al. 2001. “Oxidant Tone Regulates RANTES Gene Expression in Airway Epithelial Cells Infected with Respiratory Syncytial Virus. Role in Viral-Induced Interferon Regulatory Factor Activation.” *Journal of Biological Chemistry* 276(23): 19715–22. http://dx.doi.org/10.1074/jbc.M101526200.

Castagné, Nathalie et al. 2004. “Biochemical Characterization of the Respiratory Syncytial Virus P-P and P-N Protein Complexes and Localization of the P Protein Oligomerization Domain.” *Journal of General Virology* 85(6): 1643–53.

Chin, Ruth et al. 2007. “Modulation of MAPK Pathways and Cell Cycle by Replicating Hepatitis B Virus: Factors Contributing to Hepatocarcinogenesis.” *Journal of Hepatology* 47(3): 325–37.

Chitnis, M. M. et al. 2014. “IGF-1R Inhibition Enhances Radiosensitivity and Delays Double-Strand Break Repair by Both Non-Homologous End-Joining and Homologous Recombination.” *Oncogene* 33(45): 5262–73.

Collins, Peter L., and Gail W. Wertz. 1985. “The Envelope-Associated 22K Protein of Human Respiratory Syncytial Virus: Nucleotide Sequence of the MRNA and a Related Polytranscript.” *Journal of Virology* 54(1): 65–71.

Duan, Dongsheng et al. 1998. “Polarity Influences the Efficiency of Recombinant Adenoassociated Virus Infection in Differentiated Airway Epithelia.” *Human Gene Therapy* 9(18): 2761–76.

Elliott, Joanne et al. 2007. “Respiratory Syncytial Virus NS1 Protein Degrades STAT2 by Using the Elongin-Cullin E3 Ligase.” *Journal of Virology* 81(7): 3428–36.

Fearns, Rachel, and Peter L. Collins. 1999. “Role of the M2-1 Transcription Antitermination Protein of Respiratory Syncytial Virus in Sequential Transcription.” *Journal of Virology* 73(7): 5852–64.

Fedarko, Neal S., Masayuki Ishihara, and H. Edward Conrad. 1989. “Control of Cell Division in Hepatoma Cells by Exogenous Heparan Sulfate Proteoglycan.” *Journal of Cellular Physiology* 139(2): 287–94.

Feng, Ziheng, Lili Xu, and Zhengde Xie. 2022. “Receptors for Respiratory Syncytial Virus Infection and Host Factors Regulating the Life Cycle of Respiratory Syncytial Virus.” *Frontiers in Cellular and Infection Microbiology* 12: 1–12.

Fernandez-Capetillo, Oscar et al. 2002. “DNA Damage-Induced G2-M Checkpoint Activation by Histone H2AX and 53BP1.” *Nature Cell Biology* 4(12): 993–97.

Fuentes, Sandra et al. 2007. “Function of the Respiratory Syncytial Virus Small Hydrophobic Protein.” *Journal of Virology* 81(15): 8361–66.

Gan, Siok Wan et al. 2012. “The Small Hydrophobic Protein of the Human Respiratory Syncytial Virus Forms Pentameric Ion Channels.” *Journal of Biological Chemistry* 287(29): 24671–89.

Garcia-Barreno, Blanca, Teresa Delgado, and Jose A. Melero. 1996. “Identification of Protein Regions Involved in the Interaction of Human Respiratory Syncytial Virus Phosphoprotein and Nucleoprotein : Significance for Nucleocapsid Assembly and Formation of Cytoplasmic Inclusions.” *Journal of Virology* 70(2): 801–8.

Ghildyal, Reena, C. Baulch-Brown, J. Mills, and J. Meanger. 2003. “The Matrix Protein of Human Respiratory Syncytial Virus Localises to the Nucleus of Infected Cells and Inhibits Transcription.” *Archives of Virology* 148(7): 1419–29.

Gibson, Daniel G et al. 2009. “Enzymatic Assembly of DNA Molecules up to Several Hundred Kilobases.” *Nature Methods* 6: 343–45.

Girard, Franck, Ulrich Strausfeld, Anne Fernandez, and Ned J.C. Lamb. 1991. “Cyclin a Is Required for the Onset of DNA Replication in Mammalian Fibroblasts.” *Cell* 67(6): 1169–79.

Goldstein, Michael, Frederick A. Derheimer, Jacqueline Tait-Mulder, and Michael B. Kastan. 2013. “Nucleolin Mediates Nucleosome Disruption Critical for DNA Double-Strand Break Repair.” *Proceedings of the National Academy of Sciences of the United States of America* 110(42): 16874–79.

Gong, Yixuan et al. 2009. “High Expression Levels of Total IGF-1R and Sensitivity of NSCLC Cells In Vitro to an Anti-IGF-1R Antibody (R1507).” *Plo* 4(10): 1–11.

Gottlieb, Tanya M., and Moshe Oren. 1998. “P53 and Apoptosis.” *Seminars in Cancer Biology* 8(5): 359–68.

Grant, Gavin D, and Katarzyna M Kedziora. 2018. “Accurate Delineation of Cell Cycle Phase Transitions in Living Cells with PIP-FUCCI.” *Cell Cycle* 17(21–22): 2496–2516. https://doi.org/10.1080/15384101.2018.1547001.

Green, Gia et al. 2021. “CX3CR1 Is a Receptor for Human Respiratory Syncytial Virus in Cotton Rats.” *Journal of Virology* 95(16): 1–12.

Griffiths, Cameron D. et al. 2020. “IGF1R Is an Entry Receptor for Respiratory Syncytial Virus.” *Nature* 583(7817): 615–19. http://dx.doi.org/10.1038/s41586-020-2369-7.

Gupta, Ravi K, and Petra Mlcochova. 2022. “Cyclin D3 Restricts SARS-CoV-2 Envelope Incorporation into Virions and Interferes with Viral Spread.” *The EMBO Journal* 41(22): 1–15.

Hall, Caroline Breese. 2001. “Respiratory Syncitial Virus and Parainflueza Virus.” *New England Journal of Medicine* 344(25): 1917–28.

Hallak, Louay K., Peter L. Collins, Warren Knudson, and Mark E. Peeples. 2000. “Iduronic Acid-Containing Glycosaminoglycans on Target Cells Are Required for Efficient Respiratory Syncytial Virus Infection.” *Virology* 271(2): 264–75.

Hallak, Louay K., Dorothe Spillmann, Peter L. Collins, and Mark E. Peeples. 2000. “Glycosaminoglycan Sulfation Requirements for Respiratory Syncytial Virus Infection.” *Journal of Virology* 74(22): 10508–13.

Hanada, Norihisa et al. 2006. “Co-Regulation of B-Myb Expression by E2F1 and EGF Receptor.” *Molecular Carcinogenesis* 45(1): 10–17.

Harcourt, Jennifer et al. 2006. “Respiratory Syncytial Virus G Protein and G Protein CX3C Motif Adversely Affect CX3CR1+ T Cell Responses.” *The Journal of Immunology* 176(3): 1600–1608.

Harper, J Wade et al. 1995. “Inhibition of Cyclin-Dependent Kinases by P21.” *Molecular Biology of the Cell* 6: 387–400.

Helt, Anna Marija, and Denise A. Galloway. 2003. “Mechanisms by Which DNA Tumor Virus Oncoproteins Target the Rb Family of Pocket Proteins.” *Carcinogenesis* 24(2): 159–69.

Hosakote, Yashoda M. et al. 2009. “Respiratory Syncytial Virus Induces Oxidative Stress by Modulating Antioxidant Enzymes.” *American Journal of Respiratory Cell and Molecular Biology* 41(3): 348–57.

Hou, Shangguo, Courtney Johnson, and Kevin Welsher. 2019. “Real-Time 3D Single Particle Tracking : Towards Live Cells Spectroscopy.” *Molecules* 24(15): 2826–51.

Hou, Shangguo, and Kevin Welsher. 2019. “An Adaptive Real-Time 3D Single Particle Tracking Method for Monitoring Viral First Contacts.” *Small* 15(44): 1–9.

Huang, Feifei et al. 2019. “Phosphorylation of Nucleolin Is Indispensable to Its Involvement in the Proliferation and Migration of Non-Small Cell Lung Cancer Cells.” *Oncology Reports* 41: 590–98.

Ikeda, Hiroshi et al. 2009. “The Monoclonal Antibody NBT062 Conjugated to Cytotoxic Maytansinoids Has Selective Cytotoxicity against CD138-Positive Multiple Myeloma Cells in Vitro and in Vivo.” *Clinical Cancer Research* 15(12): 4028–37.

Jeffree, Chris E. et al. 2003. “Distribution of the Attachment (G) Glycoprotein and GM1 within the Envelope of Mature Respiratory Syncytial Virus Filaments Revealed Using Field Emission Scanning Electron Microscopy.” *Virology* 306(2): 254–67.

Jiang, Wei et al. 2013. “Influenza A Virus NS1 Induces G0/G1 Cell Cycle Arrest by Inhibiting the Expression and Activity of RhoA Protein.” *Journal of Virology* 87(6): 3039–52.

Joaquin, M., and R. J. Watson. 2003. “Cell Cycle Regulation by the B-Myb Transcription Factor.” *Cellular and Molecular Life Sciences* 60(11): 2389–2401.

Johnson, Courtney et al. 2022. “Capturing the Start Point of the Virus–Cell Interaction with High-Speed 3D Single-Virus Tracking.” *Nature Methods* 19(12): 1642–52.

Johnson, Sara M. et al. 2015. “Respiratory Syncytial Virus Uses CX3CR1 as a Receptor on Primary Human Airway Epithelial Cultures.” *PLoS Pathogens* 11(12): 1–16.

Jones, Jennifer E., Valerie Le Sage, and Seema S. Lakdawala. 2021. “Viral and Host Heterogeneity and Their Effects on the Viral Life Cycle.” *Nature Reviews Microbiology* 19(4): 272–82. http://dx.doi.org/10.1038/s41579-020-00449-9.

Kamio, Takihiro et al. 1990. “Immunohistochemical Expression of Epidermal Growth Factor Receptors in Human Adrenocortical Carcinoma.” *Human Pathology* 21(3): 277–82.

Karron, Ruth A. et al. 1997. “Respiratory Syncytial Virus (RSV) SH and G Proteins Are Not Essential for Viral Replication in Vitro: Clinical Evaluation and Molecular Characterization of a Cold-Passaged, Attenuated RSV Subgroup B Mutant.” *Proceedings of the National Academy of Sciences of the United States of America* 94(25): 13961–66.

Ke, Zunlong et al. 2018. “The Morphology and Assembly of Respiratory Syncytial Virus Revealed by Cryo-Electron Tomography.” *Viruses* 10(8).

King, Randall W, Peter K Jackson, and Marc W Kirschner. 1994. “Mitosis in Transition Review.” *Cell* 79: 563–71. https://ac.els-cdn.com/0092867494905428/1-s2.0-0092867494905428-main.pdf?_tid=b4cde802-06cf-11e8-9b54-00000aab0f26&acdnat=1517435159_9c7249e8313f19ad78260d1b3a8f8b06.

Kiss, Gabriella et al. 2014. “Structural Analysis of Respiratory Syncytial Virus Reveals the Position of M2-1 between the Matrix Protein and the Ribonucleoprotein Complex.” *Journal of Virology* 88(13): 7602–17.

Kobayashi, Junya et al. 2012. “Nucleolin Participates in DNA Double-Strand Break-Induced Damage Response through MDC1-Dependent Pathway.” *PLoS ONE* 7(11): 1–12.

Krusat, T., and H. J. Streckert. 1997. “Heparin-Dependent Attachment of Respiratory Syncytial Virus (RSV) to Host Cells.” *Archives of Virology* 142(6): 1247–54.

Krzyzaniak, Magdalena Anna et al. 2013. “Host Cell Entry of Respiratory Syncytial Virus Involves Macropinocytosis Followed by Proteolytic Activation of the F Protein.” *PLoS Pathogens* 9(4): 1–19.

Kumar-Singh, Ashish et al. 2021. “Nuclear Syndecan-1 Regulates Epithelial-Mesenchymal Plasticity in Tumor Cells.” *Biology* 10(6): 1–14.

Laiho, Marikki et al. 1990. “Growth Inhibition of Retinoblastoma by TGF-Beta Linked to Suppression Protein Phosphorylation.” *Cell* 62: 175–85.

Lehto, Jemina et al. 2021. “Targeting CX3CR1 Suppresses the Fanconi Anemia DNA Repair Pathway and Synergizes with Platinum.” *Cancers* 13(6): 1–15.

Lin, Shiaw Yih et al. 2001. “Nuclear Localization of EGF Receptor and Its Potential New Role as a Transcription Factor.” *Nature Cell Biology* 3(9): 802–8.

Ling, Zhenhua, Kim C. Tran, and Michael N. Teng. 2009. “Human Respiratory Syncytial Virus Nonstructural Protein NS2 Antagonizes the Activation of Beta Interferon Transcription by Interacting with RIG-I.” *Journal of Virology* 83(8): 3734–42.

Liu, Li et al. 2016. “Global, Regional, and National Causes of under-5 Mortality in 2000–15: An Updated Systematic Analysis with Implications for the Sustainable Development Goals.” *The Lancet* 388(10063): 3027–35. http://dx.doi.org/10.1016/S0140-6736(16)31593-8.

Liu, Wangmi et al. 2019. “CX3CL1 Promotes Lung Cancer Cell Migration and Invasion via the Src/Focal Adhesion Kinase Signaling Pathway.” *Oncology Reports* 41: 1911–17.

Lo, Hui Wen et al. 2005. “Nuclear Interaction of EGFR and STAT3 in the Activation of the INOS/NO Pathway.” *Cancer Cell* 7(6): 575–89.

Los, Georgyi V. et al. 2008. “HaloTag: A Novel Protein Labeling Technology for Cell Imaging and Protein Analysis.” *ACS Chemical Biology* 3(6): 373–382.

Low, Sarah et al. 2020. “VHH Antibody Targeting the Chemokine Receptor CX3CR1 Inhibits Progression of Atherosclerosis.” *mAbs* 12(1). https://doi.org/10.1080/19420862.2019.1709322.

Martinez, I., and J. A. Melero. 2000. “Binding of Human Respiratory Syncytial Virus to Cells: Implication of Sulfated Cell Surface Proteoglycans.” *Journal of General Virology* 81(11): 2715–22.

Martínez, Isidoro et al. 2016. “Induction of DNA Double-Strand Breaks and Cellular Senescence by Human Respiratory Syncytial Virus.” *Virulence* 7(4): 427–42.

McLellan, Jason S., William C. Ray, and Mark E. Peeples. 2013. “Structure and Function of Respiratory Syncytial Virus Surface Glycoproteins.” *Current Topics in Microbiology and Immunology* 372: 83–104.

Méndez-Callejas, Gina et al. 2017. “Antiproliferative Activity of Chloroformic Fractions from Leaves and Inflorescences of Ageratina Gracilis.” *Emirates Journal of Food and Agriculture* 29(1): 59–68.

Moghadamtousi, Soheil Z. et al. 2014. “Annona Muricata Leaves Induced Apoptosis in A549 Cells through Mitochondrial-Mediated Pathway and Involvement of NF-KB.” *BMC Complementary and Alternative Medicine* 14(1): 1–13.

Morgan, Bruce et al. 2016. “Real-Time Monitoring of Basal H2O2 Levels with Peroxiredoxin-Based Probes.” *Nature Chemical Biology* 12(6): 437–43.

Musacchio, Andrea, and Edward D. Salmon. 2007. “The Spindle-Assembly Checkpoint in Space and Time.” *Nature Reviews Molecular Cell Biology* 8(5): 379–93.

Nicholson, R. I., J. M.W. Gee, and M. E. Harper. 2001. “EGFR and Cancer Prognosis.” *European Journal of Cancer* 37(SUPPL. 4): 9.

Nisar, Hasan et al. 2023. “Hypoxia Changes Energy Metabolism and Growth Rate in Non-Small Cell Lung Cancer Cells.” *Cancers* 15(9): 1–17.

Ohtsubo, Motoaki et al. 1995. “ Human Cyclin E, a Nuclear Protein Essential for the G 1 -to-S Phase Transition .” *Molecular and Cellular Biology* 15(5): 2612–24.

Palmieri, Dario et al. 2015. “Human Anti-Nucleolin Recombinant Immunoagent for Cancer Therapy.” *Proceedings of the National Academy of Sciences of the United States of America* 112(30): 9418–23.

Pardee, A. B. 1974. “A Restriction Point for Control of Normal Animal Cell Proliferation.” *Proceedings of the National Academy of Sciences of the United States of America* 71(4): 1286–90.

Patel, J. A. et al. 1995. “Interleukin-1 Alpha Mediates the Enhanced Expression of Intercellular Adhesion Molecule-1 in Pulmonary Epithelial Cells Infected with Respiratory Syncytial Virus.” *American journal of respiratory cell and molecular biology* 13(5): 602–9.

Pleet, Michelle L. et al. 2018. “Ebola Virus VP40 Modulates Cell Cycle and Biogenesis of Extracellular Vesicles.” *Journal of Infectious Diseases* 218(S5): S365–87.

Pruessmeyer, Jessica et al. 2010. “A Disintegrin and Metalloproteinase 17 (ADAM17) Mediates Inflammation-Induced Shedding of Syndecan-1 and -4 by Lung Epithelial Cells.” *Journal of Biological Chemistry* 285(1): 555–64.

Psyrri, Amanda et al. 2005. “Quantitative Determination of Nuclear and Cytoplasmic Epidermal Growth Factor Receptor Expression in Oropharyngeal Squamous Cell Cancer by Using Automated Quantitative Analysis.” *Clinical Cancer Research* 11(16): 5856–62.

Rodrigues, Michele A. et al. 2016. “Inner Nuclear Membrane Localization of Epidermal Growth Factor Receptor (EGFR) in Spontaneous Canine Model of Invasive Micropapillary Carcinoma of the Mammary Gland.” *Pathology Research and Practice* 212(4): 340–44.

Sakaue-Sawano, Asako et al. 2008. “Visualizing Spatiotemporal Dynamics of Multicellular Cell-Cycle Progression.” *Cell* 132(3): 487–98.

Salehi, Fahimeh, Hossein Behboudi, Gholamreza Kavoosi, and Sussan K. Ardestani. 2018. “Oxidative DNA Damage Induced by ROS-Modulating Agents with the Ability to Target DNA: A Comparison of the Biological Characteristics of Citrus Pectin and Apple Pectin.” *Scientific Reports* 8(1): 1–16. http://dx.doi.org/10.1038/s41598-018-32308-2.

Sappington, Daniel R. et al. 2016. “Glutamine Drives Glutathione Synthesis and Contributes to Radiation Sensitivity of A549 and H460 Lung Cancer Cell Lines.” *Biochimica et Biophysica Acta* 1860(4): 836–843.

Savic, Miloje et al. 2023. “Respiratory Syncytial Virus Disease Burden in Adults Aged 60 Years and Older in High-Income Countries: A Systematic Literature Review and Meta-Analysis.” *Influenza and other Respiratory Viruses* 17: 1–10.

Schlender, Jörg, Birgit Bossert, Ursula Buchholz, and Karl-Klaus Conzelmann. 2000. “Bovine Respiratory Syncytial Virus Nonstructural Proteins NS1 and NS2 Cooperatively Antagonize Alpha/Beta Interferon-Induced Antiviral Response.” *Journal of Virology* 74(18): 8234–42.

Shang, Zifang, Shuguang Tan, and Dongli Ma. 2021. “Respiratory Syncytial Virus: From Pathogenesis to Potential Therapeutic Strategies.” *International Journal of Biological Sciences* 17(14): 4073–91.

Shen, Mengqin et al. 2022. “RNA-Binding Protein P54nrb/NONO Potentiates Nuclear EGFR-Mediated Tumorigenesis of Triple-Negative Breast Cancer.” *Cell Death and Disease* 13(1).

Sherr, Charles J. 1994. “G1 Phase Progression: Cycling on Cue.” *Cell* 79(4): 551–55.

Shi, Ting et al. 2017. “Global, Regional, and National Disease Burden Estimates of Acute Lower Respiratory Infections Due to Respiratory Syncytial Virus in Young Children in 2015: A Systematic Review and Modelling Study.” *The Lancet* 390(10098): 946–58.

Srikantiah, Padmini, Prachi Vora, and Keith P. Klugman. 2021. “Assessing the Full Burden of Respiratory Syncytial Virus in Young Infants in Low- And Middle-Income Countries- And Importance of Community Mortality Studies.” *Clinical Infectious Diseases* 73(Suppl 3): S177–79.

Stillman, Elizabeth A, and Michael A Whitt. 1999. “Transcript Initiation and 5-End Modifications Are Separable Events during Vesicular Stomatitis Virus Transcription.” *Journal of Virology* 87(9): 7199–7209. https://journals.asm.org/journal/jvi.

Suryawanshi, Rahul K. et al. 2021. “Dysregulation of Cell Signaling by SARS-CoV-2.” *Trends in Microbiology* 29(3): 224–37.

Swedan, Samer, Alla Musiyenko, and Sailen Barik. 2009. “Respiratory Syncytial Virus Nonstructural Proteins Decrease Levels of Multiple Members of the Cellular Interferon Pathways.” *Journal of Virology* 83(19): 9682–93.

Tai, Lihui et al. 2020. “Oxidative Stress Down-Regulates Mir-20b-5p, Mir-106a-5p and E2F1 Expression to Suppress the G1/s Transition of the Cell Cycle in Multipotent Stromal Cells.” *International Journal of Medical Sciences* 17(4): 457–70.

Tanenbaum, Marvin E. et al. 2015. “A Protein Tagging System for Signal Amplification in Gene Expression and Fluorescence Imaging.” *Cell* 159(3): 635–46.

Tawar, Rajiv G. et al. 2009. “Crystal Structure of a Nucleocapsid-like Nucleoprotein-RNA Complex of Respiratory Syncytial Virus.” *Science* 326(5957): 1279–83.

Tayyari, Farnoosh et al. 2011. “Identification of Nucleolin as a Cellular Receptor for Human Respiratory Syncytial Virus.” *Nature Medicine* 17(9): 1132–35. http://dx.doi.org/10.1038/nm.2444.

Teng, Michael N., and Peter L. Collins. 1998. “Identification of the Respiratory Syncytial Virus Proteins Required for Formation and Passage of Helper-Dependent Infectious Particles.” *Journal of Virology* 72(7): 5707–16.

Travaglione, S. et al. 2006. “Multinucleation and Pro-Inflammatory Cytokine Release Promoted by Fibrous Fluoro-Edenite in Lung Epithelial A549 Cells.” *Toxicology in Vitro* 20(6): 841–50.

Tripp, Ralph A. et al. 2001. “CX3C Chemokine Mimicry by Respiratory Syncytial Virus G Glycoprotein.” *Nature Immunology* 2(8): 732–38.

Turney, Benjamin W. et al. 2012. “Depletion of the Type 1 IGF Receptor Delays Repair of Radiation-Induced DNA Double Strand Breaks.” *Radiotherapy and Oncology* 103(3): 402–9. http://dx.doi.org/10.1016/j.radonc.2012.03.009.

Uy, Benedict, Susan R. McGlashan, and Shamim B. Shaikh. 2011. “Measurement of Reactive Oxygen Species in the Culture Media Using Acridan Lumigen PS-3 Assay.” *Journal of Biomolecular Techniques* 22(3): 95–107.

Wang, Guang Fei et al. 2017. “Oxidative Stress Induces Mitotic Arrest by Inhibiting Aurora A-Involved Mitotic Spindle Formation.” *Free Radical Biology and Medicine* 103: 177–87. http://dx.doi.org/10.1016/j.freeradbiomed.2016.12.031.

Wang, Tianzhen et al. 2011. “Hepatitis B Virus Induces G1 Phase Arrest by Regulating Cell Cycle Genes in HepG2.2.15 Cells.” *Virology Journal* 8: 1–8.

Xiong, Henry Q. et al. 2004. “Cetuximab, a Monoclonal Antibody Targeting the Epidermal Growth Factor Receptor, in Combination with Gemcitabine for Advanced Pancreatic Cancer: A Multicenter Phase II Trial.” *Journal of Clinical Oncology* 22(13): 2610–16.

Yang, Chen et al. 2020. “Nuclear IGF1R Interact with PCNA to Preserve DNA Replication after DNA-Damage in a Variety of Human Cancers.” *PLoS ONE* 15(7 July): 1–15.

Yoon, Young Kwang et al. 2010. “KRAS Mutant Lung Cancer Cells Are Differentially Responsive to MEK Inhibitor Due to AKT or STAT3 Activation: Implication for Combinatorial Approach.” *Molecular Carcinogenesis* 49(4): 353–62.

You, Li et al. 2022. “Global , Regional , and National Disease Burden Estimates of Acute Lower Respiratory Infections Due to Respiratory Syncytial Virus in Children Younger Tha.” *The Lancet* 399(10340): 2047–64. 3.

Yuan, Xiaoling et al. 2005. “G0/G1 Arrest and Apoptosis Induced by SARS-CoV 3b Protein in Transfected Cells.” *Virology Journal* 2: 1–5.

Yuan, Xiaoling et al. 2006. “SARS Coronavirus 7a Protein Blocks Cell Cycle Progression at G0/G1 Phase via the Cyclin D3/PRb Pathway.” *Virology* 346(1): 74–85.

Zhang, Liqun et al. 2002. “Respiratory Syncytial Virus Infection of Human Airway Epithelial Cells Is Polarized, Specific to Ciliated Cells, and without Obvious Cytopathology.” *Journal of Virology* 76(11): 5654–66.

Zhou, Ping et al. 2018. “Epidermal Growth Factor Receptor Expression Affects Proliferation and Apoptosis in Non-Small Cell Lung Cancer Cells via the Extracellular Signal-Regulated Kinase/MicroRNA 200a Signaling Pathway.” *Oncology Letters* 15(4): 5201–7.

Zhu, Li et al. 2021. “Multiple RNA Virus Matrix Proteins Interact with SLD5 to Manipulate Host Cell Cycle.” *Journal of General Virology* 102: 1–18.

Zielonka, Jacek, and B. Kalyanaraman. 2010. “Hydroethidine- and MitoSOX-Derived Red Fluorescence Is Not a Reliable Indicator of Intracellular Superoxide Formation: Another Inconvenient Truth.” *Free Radical Biology and Medicine* 48(8): 983–1001. http://dx.doi.org/10.1016/j.freeradbiomed.2010.01.028.

Zielonka, Jacek, Jeannette Vasquez-Vivar, and Balaraman Kalyanaraman. 2008. “Detection of 2-Hydroxyethidium in Cellular Systems: A Unique Marker Product of Superoxide and Hydroethidine.” *Nature Protocols* 3(1): 8–21.

Extended data

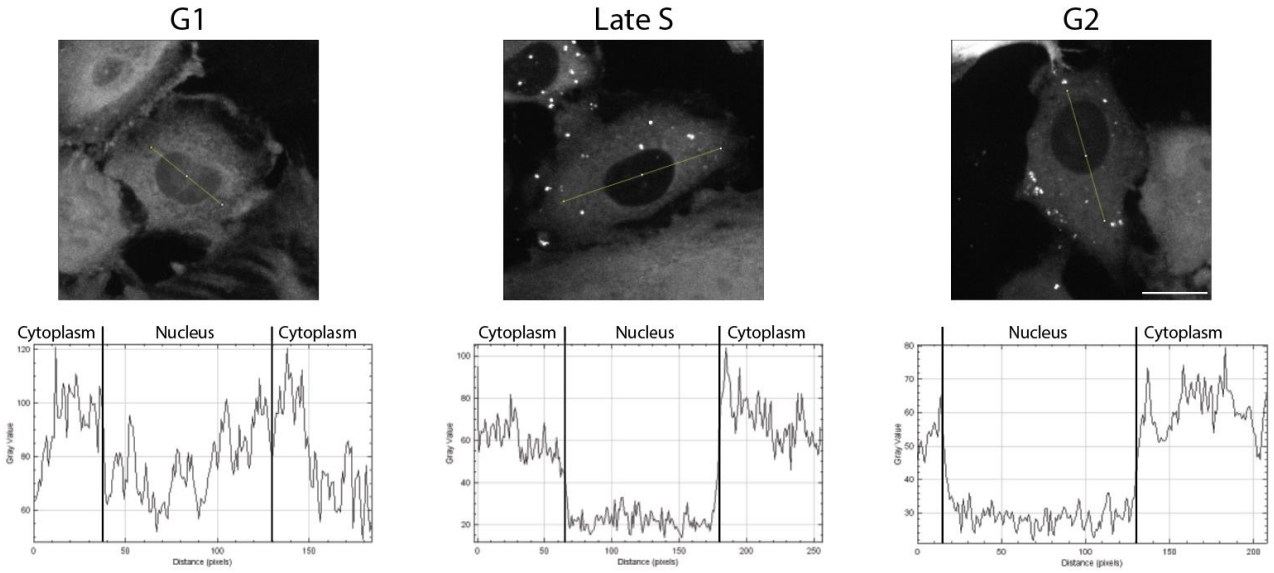

Supplementary Figure 1. P-STAb-PIP-FUCCI$^{G/R}$ ***nuclear PIP signal is distinguishable across different cell cycle phases.*** *Line profiles depicting the variation in PIP fluorescent signal intensity across a selected* P-STAb-PIP-FUCCI$^{G/R}$ *cell. Lines were drawn across the cell center to ensure the capture of the cytosol and nucleus. Scalebar = 10µm.*

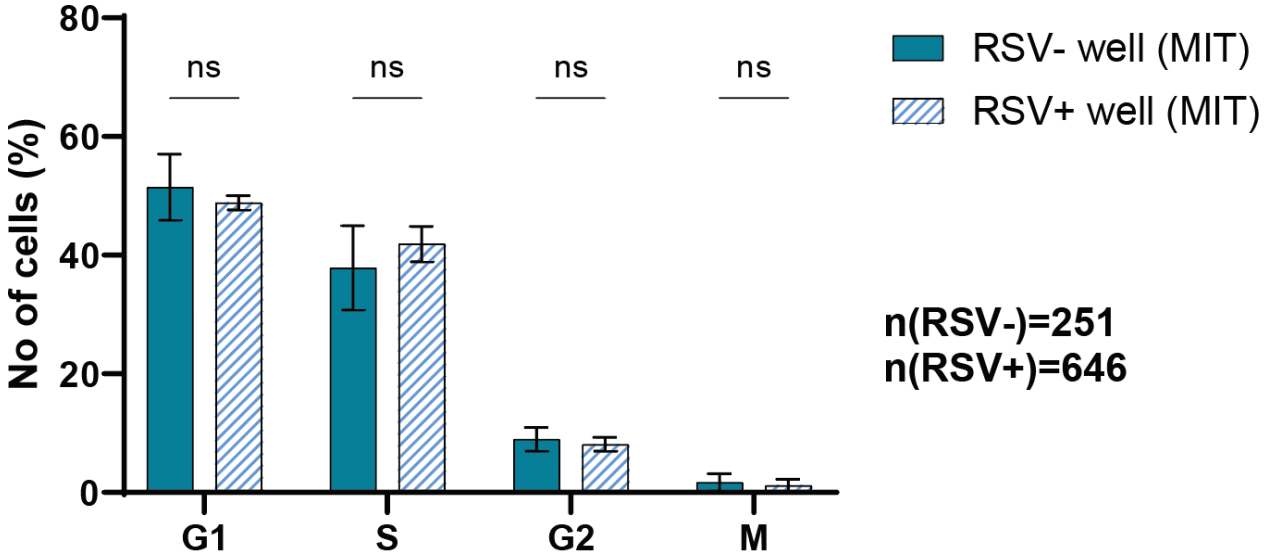

Supplementary Figure 2. The cell cycle phase fractions between RSV- and RSV+ populations at median infection time match. *Bar graph displaying the cell cycle phase fractions of RSV-infected (RSV+) and RSV- control cells at replicate-specific median infection times (MIT). The outlined results represent the mean±SD of distinct biological replicates (n=3). Displayed n values depict the number of cells analyzed per condition.*

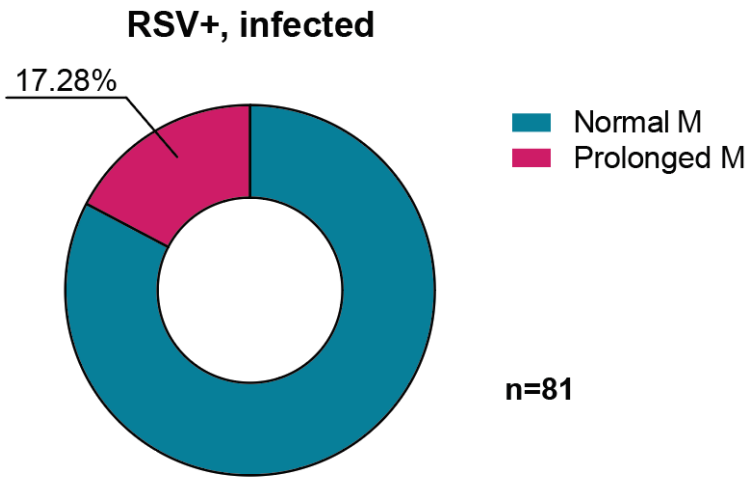

Supplementary Figure 3. A portion of RSV-infected cells displayed prolonged mitosis. *Pie chart depicting the percentage of infected P-STAb-PIP-FUCCI$^{G/R}$ cells that were presented with M phases that were longer than the established normal of xxx h. n values the total number of infected cells where mitosis was observed.*